Journal of Controlled Release 358 (2023) 43–58

Contents lists available at ScienceDirect

Journal of Controlled Release

journal homepage: www.elsevier.com/locate/jconrel

Functionalized retinoic acid lipid nanocapsules promotes a two-front attack on inflammation and lack of demyelination on neurodegenerative disorders

Rui Pedro Moura [a,b,c,d], Eva Daniela Carvalho [a,b,e], Cláudia Martins [a,b,c], Anne des Rieux [f], Ana Paula Pêgo [a,b,e], Bruno Sarmento [a,b,c,d,*]

[a] i3S – Instituto de Investigação e Inovação em Saúde, Universidade do Porto, Rua Alfredo Allen 208, 4200-135 Porto, Portugal
[b] INEB – Instituto de Engenharia Biomédica, Universidade do Porto, Portugal
[c] ICBAS – Instituto de Ciências Biomédicas Abel Salazar, Universidade do Porto, Rua de Jorge Viterbo Ferreira 228, 4050-313 Porto, Portugal
[d] IUCS – Instituto Universitário de Ciências da Saúde, CESPU, Rua Central de Gandra 1317, 4585-116 Gandra, Portugal
[e] FEUP – Faculdade de Engenharia da Universidade do Porto, Universidade do Porto, Dr. Roberto Frias, 4200-465 Porto, Portugal
[f] Advanced Drug Delivery and Biomaterials, Louvain Drug Research Institute, University of Louvain, 1200 Brussels, Belgium

ARTICLE INFO

Keywords:
Dual therapy
Nanoparticles
Neurodegeneration
Myelination

ABSTRACT

Demyelinating disorders, with a particular focus on multiple sclerosis (MS), have a multitude of detrimental cognitive and physical effects on the patients. Current treatment options that involve substances promoting remyelination fail in the clinics due to difficulties in reaching the central nervous system (CNS). Here, the dual encapsulation of retinoic acid (RA) into lipid nanocapsules with a nominal size of 70 nm, and a low PdI of 0.1, coupled with super paramagnetic iron oxide nanoparticles (SPIONs) was accomplished, and joined by an external functionalization process with a transferrin-receptor binding peptide. This nanosystem showed a 3-fold improved internalization by endothelial cells compared to the free drug, ability to interact with oligodendrocyte progenitor cells and microglia, and improvements in the permeability through the blood-brain barrier by 5-fold. The lipid nanocapsules also induced the differentiation of oligodendrocyte progenitor cells into more mature, myelin producing oligodendrocytes, as evaluated by high-throughput image screening, by 3–5-fold. Furthermore, the ability to tame the inflammatory response was verified in lipopolysaccharide-stimulated microglia, suppressing the production of pro-inflammatory cytokines by 50–70%. Overall, the results show that this nanosystem can act in both the inflammatory microenvironment present at the CNS of affected patients, but also stimulate the differentiation of new oligodendrocytes, paving the way for a promising platform in the therapy of MS.

1. Introduction

Demyelinating disorders are characterized by a progressive loss of the insulating layer that enwraps neurons in the central nervous system (CNS), known as myelin, and typically resulting in significantly impaired neuronal communication [1]. These diseases are characterized by a progressive development of lesions with loss of function of critical cellular players in the homeostasis, such as oligodendrocytes, microglia, and astrocytes [2]. Oligodendrocytes in particular are the cells that produce the myelin in the CNS [3]. Oligodendrocyte disfunction or direct myelin destruction are the main issues in demyelinating disorders, such as multiple sclerosis (MS) [4], which typically leads to significant impairments in the quality of life of individuals. MS particularly stems from a multifactorial ethology, wherein the underlying cause is still not fully understood, where a targeted immune reaction occurs against the myelin, leading to the formation of a persistent inflammatory state. Different theories have been put forward, ranging from genetic, environmental or even infectious due to molecular mimicry. At early stages of the disease, remyelination can occur when oligodendrocyte-progenitor cells (OPCs) are mobilized to a lesion area where focal demyelination is occurring, and undergo differentiation into mature, myelin producing oligodendrocytes [5]. In late chronic states of MS, oligodendrocyte progenitor cells (OPCs) or oligodendrocytes are not able to restore the destroyed myelin anymore. Additionally, the formation of a glial scar within the lesion sites not only contributes to the failure of the regeneration process but also to further neurodegeneration [6].

Therapeutic approaches currently in clinical practice for MS focus

* Corresponding author at: i3S – Instituto de Investigação e Inovação em Saúde, Universidade do Porto, Rua Alfredo Allen 208, 4200-135 Porto, Portugal.
E-mail address: bruno.sarmento@i3s.up.pt (B. Sarmento).

https://doi.org/10.1016/j.jconrel.2023.04.034
Received 9 February 2023; Received in revised form 14 March 2023; Accepted 18 April 2023
Available online 28 April 2023

primarily on disease-modifying therapies (*e.g.*, dimethyl fumarate, fingolimod, teriflunomide) that attempt to control the inflammatory environment at the CNS in order to reduce the rate of demyelination and symptom flare-ups [7,8]. The main limitation behind the lack of therapeutic options that focus on remyelination stems from the poor bioavailability of candidate drugs to the CNS due to the presence of the blood-brain barrier (BBB) [9]. In order to improve therapeutic outcomes in demyelinating disorders, particularly MS, alternative therapies must be considered to fully harness the power of remyelinating agents.

Lipid nanocapsules (LNCs) are a versatile nanosystem that can be rapidly developed by a process devoid of organic solvents that follows a phase-inversion methodology [10]. LNCs are made up of Food and Drug Administration approved excipients for all routes of administration and can promote the encapsulation of a plethora of different therapeutics [11,12]. The preparation process is simple to scale-up and the LNCs exhibit long-term stability when stored at 4 °C, highlighting the potential for clinical application of these particles [12]. Due to their lipidic nature, it is also quite simple to encapsulate lipid fluorescent tracers to track the LNC in multiple assays that require particle tracking [13]. Furthermore, the surface of the LNC can be modified in order to carry targeting agents that promote an increased accumulation of the LNCs in target tissues or cells [14]. With a particular interest in improving the bioavailability to the CNS in the case of MS, targeting the transferrin receptor (TfR) through the use of either antibodies or peptides has been the preferred option, due to the overexpression of the receptor at the BBB [14]. TfR is a promising target since it is exclusively expressed by endothelial cells of the brain capillaries thus preventing significant off-target effects [15]. For instance, a previously reported TfR-targeted peptide (TfRp) (Thr-His-Arg-Pro-Pro-Met-Trp-Ser-Pro-Val-Trp-Pro-Cys) effectively showed the ability to promote polymeric nanoparticles with a significant improvement in permeability through a BBB *in vitro* model [16,17] and BBB cell uptake [18].

Retinoic acid, particularly all-trans retinoic acid (RA), is a widely used agent in many differentiation protocols for neural stem cells [19]. Additionally, RA can also promote alterations in the immune response caused by microglia [20] and act in a pro-regenerative way at the CNS [20]. Studies have already demonstrated that RA can induce the differentiation of neural stem cells into mature neuronal cells and is required to stimulate the differentiation of OPCs into mature oligodendrocytes [21–23]. As RA is able to act both on the immune response and to stimulate progenitor cell differentiation, we postulate that RA would be an ideal candidate to tackle the two pillars of MS, in this case, both the pro-inflammatory microenvironment due to the targeted destruction of myelin sheaths by activated immune cells, and the lack of remyelination of lesions sites in MS. As RA suffers from premature degradation and chemical instability, LNCs could be a prime delivery platform to allow RA to reach the CNS in therapeutically ideal concentrations to fully harness its therapeutic potential. To ensure that the LNC preferentially recognize the TfR expressed primarily at the BBB interface, the formulations were co-loaded with super paramagnetic iron-oxide nanoparticles (SPIONs) to promote magnetic guidance of the LNC towards the CNS by the presence of an external magnetic field close to the head of the patient. Different works have focused on the use of SPIONs and other drugs encapsulated within one nanostructure to achieve magnetic targeting or their potential to aid with the imaging of certain conditions [24,25]. The SPIONs are also commercially available and considered safe for administration, and are externally stabilized by the presence of oleic acid to grant them the necessary hydrophobicity to ensure their encapsulation within the LNC.

Herein, TfRp functionalized SPION-LNC RA were developed to achieve high rates of brain permeability and to significantly improve the pharmacokinetic properties of RA. The goal of this work was to assess the developed functionalized LNC on their ability to cross the BBB, and to interact with both OPCs and microglia in order to promote the production of new myelin and to control the inflammatory environment, that is characteristic in MS. The impact on cell metabolic activity and potential biological interactions of the TfRp-SPION-LNC RA was evaluated in microglia, OPCs and endothelial cells. Then, TfRp-SPION-LNC RA were evaluated for their potential to stimulate OPCs differentiation, as well as the potential to control the inflammatory response in an lipopolysaccharide (LPS)-activated microglia model.

2. Materials and methods

2.1. Materials

Transferrin-receptor binding peptide (Thr-His-Arg-Pro-Pro-Met-Trp-Ser-Pro-Val-Trp-Pro-Cys) was purchased from GenScript (Piscataway, NJ, USA); crosslinker (NH_2-PEG-Mal, PEG of 5 kDa) from Biochempeg (Watertown, MA, USA) Labrafac® was kindly provided by Gattefosse SA (Saint-Priest, France); Phospholipon® 80H Lipoïd® was purchased from Lipoid Gmbh (Ludwigshafen, Germany); Kolliphor® HS 15 was gifted from BASF (Ludwigshafen, Germany); DiD solid; DiIC18(5) solid and phalloidin-alexa fluor 488 was bought from Alfagene (Lisboa, Portugal); iron oxide(II,III), magnetic nanoparticles were acquired from Laborspirit, lda (Lisboa, Portugal); retinoic acid, millex-HV Syringe Filter Unit, 0.45 μm, sodium chloride, sodium hydroxide, sulfanilamide, glycerin, Tween® 80, hydrocortisone, ascorbic acid, 4-(2-hydroxyethyl)-1-piperazineethanesulfonic acid (HEPES), basic fibroblast growth factor (bFGF), 3-(4,5-dimethylthiazol-2-yl)-2,5-diphenyltetrazolium bromide (MTT), N-(1-Naphthyl)ethylenediamine dihydrochloride, poly(L-lysine), rabbit anti-Olig2, mouse anti α-tubulin, alexafluor 488, 546 and 647, paraformaldehyde egtazic acid, magnesium chloride, piperazine-*N*,*N*′-bis(2-ethanesulfonic acid), resazurin, sodium nitrite and sodium azide were purchased from Sigma (St. Louis, MO, USA); Hoechst was acquired from Molecular Probes (Eugene, OR, USA); DMSO from VWR (West Chester, PA, USA); rat anti-myelin basic protein was bought from AbD serotec (Raleigh, NC, USA); endothelial basal medium 2 (EBM-2) and high glucose with UltraGlutamine™ Dulbecco's Modified Eagle medium (DMEM) from Lonza (Basel, Switzerland); for high-pressure liquid chromatography (HPLC) analysis, trifluoroacetic acid (TFA) purchased from Acros Organics (USA) and Acetonitrile HPLC Gradient Grade purchased from Fisher Scientific (UK) were used; Triton X-100 from Spi-Chem (West Chester, PA, USA); fetal bovine serum (FBS), penicillin-streptomycin, chemically defined lipid concentrate, rat tail collagen type I and acetic acid, from Gibco (Waltham, MA, USA); ethanol from Valente e Ribeiro, Lda (Lisbon, Portugal); IL-6, Il-10 and TNF-α complete ABTS development kits were purchased from Peprotech (Rocky Hill, NJ, USA); E.coli O111:B4 LPS was acquired from Invivogen (San Diego, CA, USA); Hank's Balanced Salt Solution (HBSS) without calcium or magnesium supplemented with trypsin (0.0025% *w/v*) and 0.001 $mg.mL^{-1}$ DNAse I was purchased from Applichem GmbH (Darmstadt, Germany); normal donkey serum was acquired from Biosource (San Diego, CA, USA) Ultrapure water was prepared in-house.

Immortalized human cerebral microvascular endothelial cell line (hCMEC/D3 cell line) was purchased from Cedarlane (Hornby, ON, Canada), immortalized rat microglia cell line (BV-2) was kindly provided by Anne des Rieux, PhD from Université Catholique de Louvain, Belgium.

2.2. Lipid nanocapsules manufacture

LNC were prepared following the protocol previously developed by Heurtault et al. [10]. In brief, Kolliphor® HS 15 (0.450 g), Phospholipon® 80H (0.045 g), NaCl (0.060 g), Labrafac® (0.600 g) and water (1.975 g) were mixed with gentle magnetic stirring at 40 °C for 10 min. Afterwards, the solution was slowly heated until 90 °C and cooled to 60 °C a total of three times. During the last cycle, a rapid shock with cold water (10 g, at 4 °C) was added at 75–77 °C under high-speed stirring. For RA loaded LNC, 250 μL of previously dissolved RA in DMSO (10 $mg.mL^{-1}$) was added at 79–81 °C at the last heating/cooling cycle. For SPIONs addition, 100 μL of a stock solution at 5 $mg.mL^{-1}$ in toluene was

added simultaneously with RA. For blank LNC, 250 μL of water was added instead. Afterwards, the LNC were centrifuged at 3200 x*g* to remove all the unreacted lipids and then filtered through a 0.45 μm syringe filter. This process was replicated with a 10-fold increase in excipients as a pilot scale-up study (LNC RA 10×). For LNC DiD, 0.3 mg of DiD (1 mg.mL^{-1} in absolute ethanol) was previously dissolved in Labrafac® before the excipients were mixed, and then the same process mimicked. All formulations were then stored at 4 °C until further use.

2.2.1. Surface functionalization of lipid nanocapsules with a transferrin-receptor binding peptide

Transferrin-receptor binding peptide LNC (TfRp-LNC) were modified post-manufacturing by a two-step process. Firstly, NH_2-PEG-maleimide was introduced on to the shell of the LNC *via* a transacylation reaction with Kolliphor® HS 15 [26]. 1 μM NH_2-PEG-maleimide was added to 2 mL of LNC (molar ratio malameide:Kolliphor 1:90), followed by 10 mL of NaOH 10 M. This reaction took place at 25 °C for 15 min and was then stopped by an acidic glycine buffer. The NH_2 reacts with the hydroxystearic acid present on Kolliphor® HS 15 and creates an amide bond with the LNC [27]. The unreacted NH_2-PEG-malameide was separated by dialysis for 48 h (dialysis membrane MWCO 10 kDa), with water changes at 2, 4, 24 and 48 h. The second step consisted of the reaction of the maleimide with the terminal cysteine of the transferrin-receptor binding peptide (TfRp) (Thr-His-Arg-Pro-Pro-Met-Trp-Ser-Pro-Val-Trp-Pro-Cys). 500 μL of 0.5 mg.mL^{-1} TfRp was added to the LNC (molar ratio 1:2.39) and kept under stirring at 150 rpm for 2 h, vortexing every 30 min. Afterwards, 2 mM of NaCl and 0.1 mM of Cysteine hydrochloride were added to block all the unreacted maleimide at the surface of the LNC. The solution was then purified from unattached TfRp by dialysis for 48 h with water changes at 2, 4, 24 and 48 h.

2.3. Physico-chemical characterization of lipid nanocapsules

The physico-chemical properties of the LNC were assessed using a Malvern Zetasizer Nano ZS (Malvern Instruments). To measure the average size and polydispersibility index (PdI), the samples were diluted in 1/100 in deionized water. To evaluate the zeta-potential, the samples were diluted at the same concentration in NaCl 10 mM. These analyses were repeated at 3, 6 and 9 months to assess long-term stability of the nanosystem.

An *in vitro* release study was performed to validate the release profile of RA from the matrix of the LNC, compared to the diffusion profile of RA under simulated biological media conditions. Briefly, 5 mL of TfRp-SPION-LNC RA was placed in a dialysis membrane (MWCO: 10 kDa) and submerged in 30 mL of PBS pH 7.4 with 1% Tween-80, and compared to the free RA through 8 days. At selected timepoints, 1 mL of the external phase was removed and quantified to verify the released drug from within the membrane, with an equal amount of the external phase being added to match.

Transmission electron microscopy (TEM) characterization of the LNC was performed on using a JEOL JEM-1400 microscope. Samples were prepared by adding 10 μL of the suspension of the LNC onto a 300-mesh nickel grid and stained with 1% uranyl acetate. Elemental analysis through energy – dispersive X-ray spectroscopy (STEM-EDS) was performed to search for the presence of sulphur in functionalized batches.

Scanning electron microscopy (SEM) exam was performed using a High-resolution Scanning Electron Microscope with X-Ray Microanalysis and CryoSEM: JEOL JSM 6301F/ Oxford INCA Energy 350/ Gatan Alto 2500. The samples were rapidly cooled (plunging it into sub-cooled nitrogen – slush nitrogen) and transferred under vacuum to the cold stage of the preparation chamber. Afterwards, samples were fractured, sublimated ('etched') for 180 s. at −90 °C, and coated with Au/Pd by sputtering for 90 s. CryoSEM evaluations were carried out at a temperature of −150 °C.

The association efficiency of RA was measured by the direct method. The LNC were destroyed by dissolution in methanol (1/20) to release the encapsulated RA. RA was then quantified by Reverse-phase High-performance Liquid Chromatography using a HPLC column-Xterra (3.5 μm) RP18. The mobile phase was composed of water and acetonitrile solution with 0.01% Trifluoroacetic acid (TFA) in a 15:85 ratio. The method was run in an isocratic mode with a flow rate of 1 mL/min and an injection volume of 20 μL. The encapsulation efficiency was calculated with the following equation:

$$AE\% = \frac{Measured\ retinoic\ acid}{Total\ added\ retinoic\ acid} \times 100.$$

The total amount of SPIONs was assessed by the *ortho*-phenanthroline method similarly using the direct method, where the LNC were destroyed by dissolution in methanol (1/20) to release the SPIONs entrapped within the matrix of the LNC [28], and the SPIONs in solution was then calculated by the following equation:

$$AE\% = \frac{Measured\ SPIONs}{Total\ added\ SPIONs} \times 100$$

2.4. Cell culture

2.4.1. Immortalized endothelial human cell culture (hCMEC/D3)

Immortalized human cerebral microvascular endothelial cells (hCMEC/D3) were grown in tissue cultured flasks, in EBM-2 supplemented medium with heat-inactivated FBS (5%, *v*/v), penicillin-streotomycin (1%, v/v), hydrocortisone (1.4 μM), ascorbic acid (5 μg.mL^{-1}), chemically defined lipid concentrate (1/100, v/v), HEPES (10 mM) and bFGF (1 ng.mL^{-1}). The bFGF was always added extemporaneously in the cell culture medium. Cells were sub-cultured every 5–6 days using trypsin–EDTA to detach them from the flasks. The culture medium was replaced every other day. Cells between the passages 48–58 were used.

2.4.2. Immortalized microglia rat cell culture (BV-2)

Immortalized rat microglia cell was grown in Dulbecco's modified eagle medium (DMEM) supplemented with FBS (5%, *v*/v), penicillin-streotomycin (1%, v/v) Cells were sub-cultured every 3–4 days using trypsin–EDTA to detach them from the flasks. The culture medium was replaced every other day. Cells between the passage 25–36 were used.

2.4.3. Primary rat oligodendrocyte precursor cell culture (OPCs)

All procedures involving animals and their care were performed in agreement with institutional ethical guidelines, the EU directive (2010/63/EU) and Portuguese law (DL 113/2013). Experiments described here had the approval of Portuguese Veterinary Authorities. Animals had free access to food and water, being kept under a 12-h light/12-h dark cycle.

Primary cultures of OPCs were obtained as previously described [29,30]. Briefly, mixed glial cultures were isolated from the brains of P0-P2 Wistar Han rats. Isolated cortices were digested in Hank's Balanced Salt Solution (HBSS) without calcium or magnesium supplemented with trypsin (0.0025% *w*/*v*) and 0.001 mg.mL^{-1} DNAse I for 15 min at 37 °C. Dissociated cortices were cultured in poly(L-lysine) (PLL) coated 75 cm^2 flasks and maintained in Dulbecco's Modified Eagle Medium (DMEM) supplemented with 10% (*v*/v) heat-inactivated (30 min, 56 °C) FBS and 1% (v/v) penicillin-streptomycin. When confluence was reached (~12 days) the flasks were shaken overnight on an orbital shaker (220 rpm) at 37 °C to remove loosely attached microglia and OPCs. OPCs were further purified by a differential selective adhesion step by seeding cells in suspension into non-tissue culture treated petri dishes for 2 h to remove microglial cells. OPCs were then seeded on PLL pre-coated glass coverslips and maintained for 18 h in OL SATO medium which was composed by DMEM medium supplemented with transferrin (0,1 mg.mL^{-1}), bovine serum albumin (BSA) (0.1 mg.mL^{-1}), putrescin (16 μg.mL^{-1}), progesterone (60 ng.mL^{-1}), thyroxine (40 ng.mL^{-1}), sodium selenite (40 ng.mL^{-1}), triiodo-L-thyroxine (30 ng.mL^{-1}), insulin (5 μg.mL^{-1}) and 0.5% heat-inactivated (30 min, 56 °C) FBS. After 18 h, the media was

discarded and replaced by OL SATO with LNC, free RA, TfRp-LNC RA and TfRp-SPION-LNC RA. After 4 h, the media was discarded again and replaced by fresh OL SATO. Microglia and a small percentage of astrocytes were present in the cultures but did not influence the normal behavior and differentiation of OPCs. Cells were evaluated at day 2 and 5 of differentiation.

2.5. Evaluation of the effect of lipid nanocapsules on cell metabolic activity

Cellular metabolic activity was assessed either through the 3-(4,5-dimethylthiazol-2-yl)-2,5-diphenyltetrazolium bromide (MTT) reduction (microglia and endothelial cells) or the resazurin assay (OPCs). Cells were seeded in a 96-well plate at a density of 6.25×10^4 viable cells/cm^2 for hCMEC/D3 and 3.13×10^4 viable cells/cm^2 for BV-2. The cells were then incubated for 48 h (hCMEC/D3) and 24 h (BV-2) and then the medium was removed, and the cells were washed twice with phosphate buffered saline (PBS). Afterwards, the cells were incubated with different concentrations of empty LNC, free drug and TfRp-LNC RA, for 4 and 24 h Afterwards, hCMEC/D3 and BV-2 cells were incubated with MTT solution (0.5 mg.mL^{-1} in medium) for 3 h. Lastly, the MTT was removed and DMSO was added to dissolve the formazan crystals formed after a gentle room temperature (RT) shake. The absorbance was measured at 590 and 630 nm. The metabolic activity was calculated as a percentage compared to the cells incubated only with plain medium (EBM-2 and DMEM, respectively) and incubated with triton X-100 (1% *v*/v, in PBS). Data was referenced to a 70% cell viability threshold according to ISO 10993–5 [31].

OPC metabolic activity was inferred through the resazurin methodology at day 2 and 5 of differentiation. The cells were incubated with 10% (*v*/v) solution of resazurin diluted in OL SATO and cells for 3 h. Afterwards, 100 μL was transferred to a dark 96-well plate Cell metabolism was inferred by measuring the levels of produced resofurin, which is a molecule produced by the reduction of resazurin (redox-sensitive fluorescent dye) [32]. Fluorescence was measured at an excitation of 530 nm and emission of 590 nm using a fluorometer Synergy Mx (BioTeK Instruments, GenX software).

2.6. Evaluation of lipid nanocapsules-cell interaction

The ability by the target cells to interact with and internalize the LNC is of paramount importance to ensure the biological activity of RA. To quantify the internalization by endothelial cells of the BBB, hCMEC/D3 were seeded in a 6-well plate at a density of 6.25×10^4 viable cells/cm^2 and were left to adhere overnight. The cells were then washed twice with PBS and then incubated with TfRp-SPION-LNC DiD, LNC DiD and TfRp-SPION-LNC DiD + TfRp for 1 h and 4 h (data not shown). After the incubation, the cells were washed twice and detached by trypsin-EDTA. The cells were then fixed with PFA 4% in PBS for 20 min (RT), washed twice with PBS and resuspended in PBS filtered through a 70 μm mesh and placed in cytometer tubes. The fluorescence intensity was analyzed with a flow cytometer (Accuri).

To obtain a qualitative analysis of the interaction with hCMEC/D3 cells, they were seeded in glass cover slips in a 24-well plate at a density of 3.1×10^5 viable cells/cm2. After 48 h in culture, the medium was removed and the cells were washed twice with pre-warmed PBS, and then incubated with TfRp-LNC DiD or LNC DiD. Additionally, cells were pre-treated with TfRp before incubation with TfRp-LNC DiD to evaluate whether targeted-LNC uptake is specific of TfR. The equivalent dye concentration encapsulated within the LNC was set to 1 μg.mL^{-1}. After 1 h incubation (37 °C, 5% CO_2), the cells were washed and fixed with 4% PFA. Afterwards, the cells were stained with Alexa Fluor 488 nm phalloidin and hoescht (405 nm) and mounted with fluoromount mounting media. Afterwards the cells were observed with a laser scanning confocal microscope (Leica SP5, 405 nm for Hoescht, 520 nm for phalloidin and 644 nm for DiD).

For BV-2, the cells were seeded at a density of 1×10^5 viable cells/cm^2, and the same protocol from above was applied. After 4 h of incubation the cells were washed again and fixed with 4% PFA and permeabilized and blocked in PBS containing 5% (*v*/v) normal donkey serum (NDS) and 0.3% (v/v) Triton X-100. The primary antibodies were diluted in PBS and incubated overnight in a humid chamber at 4 °C. The following primary antibodies were used: rabbit anti-Iba-1 (1:500), mouse anti-alpha tubulin (1:2000). The following day, secondary antibodies Alexa-Fluor 488 and 568 (1:1000) were applied for 1 h at RT and subsequently treated for nuclear counterstaining at RT with Hoechst at 2 μL.mL^{-1}, and subsequently mounted with fluoromount mounting media. The cells were then observed by scanning confocal microscope (Leica SP5, 405 nm for Hoescht, 488 for Iba-1 and 568 for tubulin.

The OPCs were seeded on glass coverslips in a 24-well plate at a density of 3.1×10^4 viable cells/cm^2. After 24 h for cellular adhesion, the medium was removed, and the cells were treated with TfRp-SPION-LNC DiD at an equivalent encapsulated dye concentration of 0.1 μg.mL^{-1}. After 4 h of incubation, the medium with the LNC was removed and fresh medium was added. At day 2 and 5 of differentiation, the cells were fixed with 4% (*v*/v) paraformaldehyde containing microtubule stabilizers [29] (MP-PFA, 4% PFA with the addition of 65 mM piperazine-*N*,*N*′-bis(2-ethanesulfonic acid) (PIPES), 25 mM of HEPES, 10 mM of egtazic acid (EGTA) and 3 mM $MgCl_2$, for 15 min and further permeabilized and blocked in PBS containing 5% (v/v) NDS and 0.3% (v/v) Triton X-100. Primary antibodies were diluted in PBS containing 1% (v/v) NDS and 0.15% (v/v) Triton X-100 and incubated overnight in a humid chamber at 4 °C. The following primary antibodies were used: rabbit anti-Olig2 (1:400), rat anti-MBP (1:100). Secondary antibodies Alexa-Fluor 488 and 568 were applied for 1 h at RT and subsequently treated for nuclear counterstaining at RT with Hoechst at 2 μL.mL^{-1}. Afterwards, the cells were mounted using Fluoromount™ mounting media. The cells were then observed with scanning confocal microscope (Leica SP5, 405 nm for Hoescht, 488 nm for Olig2, 568 nm for myelin basic protein (MBP) and 644 nm for DiD). Cell images were analyzed using Fiji ImageJ software version 2.3.0.

2.7. Permeability assays in a blood-brain barrier model

A BBB *in vitro* model, based on a transwell system, was adapted from a previous work [16] to evaluate the permeability of the LNC nanoparticles. Briefly, 2.5×10^4 viable cells/cm^2 of hCMEC/D3 cells (500 μL of medium) were seeded in 12-well plates in transwell® cell culture inserts with a 1 μm pore size (apical side). Before the seeding, the inserts were coated with 90 μL of a 50 μg.mL^{-1} rat tail collagen type I previously diluted in an acetic acid solution (0.02 M) for 1 h (37 °C, 5% CO_2). Afterwards, inserts were washed twice with PBS pH 7.4. The basolateral side was filled with 1.5 mL of medium. The system was maintained in the incubator at 37 °C with 5% CO_2 for 8 days, and medium was changed every 2 days. The hCMEC/D3 cells monolayer became confluent at the day 8 after seeding, which was the day appropriate to perform the permeability study. The integrity of the cell monolayer was checked every other day by monitoring the trans endothelial electric resistance (TEER) using an endothelial Volt–Ohm meter (Millicell® ER S-2; Merck Millipore, Billerica, MA, USA). The resistance value of an empty filter with only media was subtracted from each measurement.

The permeability experiment was performed in the apical-to-basolateral direction. After removing the cell culture medium, the basolateral compartment was filled with 1.5 mL of HBSS, ensuring sink conditions. Regarding the apical compartment, 500 μL of RA at 0.1 and 1 μg.mL^{-1}, in the free form or loaded on either TfRp-SPION-LNC or non-functionalized LNC, diluted in HBSS were added. Then, the assay was conducted at 37 °C using an orbital shaker incubator (100 rpm). At different time points (60, 120, 180 and 240 min), 200 μL samples were taken from the basolateral side, and the same volume of pre-heated HBSS was added to replace the withdrawn volume. At the last time-point, the monolayer was disrupted with the presence of 1% Tween-80

in order to lyse the cells to quantify intracellular RA. The integrity of the cell monolayer was checked during the permeability experiment by monitoring the TEER. The apparent permeability coefficient, Papp (cm. s-1), measures drug permeability across the cell monolayer, and is calculated according to the following equation:

$$P_{app} = \frac{dQ}{dt} \times \frac{1}{A \times C_0}$$

where dQ (μg) is the amount of drug that permeated from the apical to the basolateral compartment during the incubation time t (s), A is the surface area of the transwell® insert (cm^2) and C_0 the initial concentration of the drug on the apical side ($\mu g.mL^{-1}$). The samples were analyzed by the method described above for HPLC, with some adaptations proposed by us. 20 μL of each sample was separated on an HPLC Vanquish (Thermo Fischer Scientific, Bremen, Germany). The column was a Accucore RP-MS column (Thermo Fischer Scientific, Bremen, Germany) 2.6 μm particle size and dimensions 100 mm ID x 2.1 mm. The samples were eluted in isocratic conditions with 15% solvent A (miliQ water with 0.1% *v*/v formic acid) and 85% of solvent B (acetonitrile with 0.1% v/v formic acid) during 15 min at a flow rate of 0.350 mL/min.

The Analysis was done on an Orbitrap Exploris 120 mass spectrometer (Thermo Fischer Scientific, Bremen, Germany) controlled by Orbitrap Exploris Tune Application 2.0.185.35 and Xcalibur 4.4.16.14. The capillary voltage of the electrospray ionization source (ESI) was set to 3.5 kV. The capillary temperature was 300 °C. The sheath gas, auxiliary and sweep gas flow rate were at 50, 10 and 1 (arbitrary unit as provided by the software settings). Single ion monitoring (SIM) was used to detect RA (300.2084 Da). The resolution of MS scan was 60,000. Data dependent MS/MS was performed on HCD using nitrogen as gas with collision energy settings of 30 V.

MS data handling software (Xcalibur QualBrowser software, Thermo Fischer Scientific) was used to search extrapolate the concentration of RA by their *m/z* value and MS/MS value.

2.8. Anti-inflammatory action of lipid nanocapsules

To investigate if TfRp-SPION-LNC RA were able to adequately suppress the microglia activation that occurs in the CNS in demyelinating disorders, BV-2 were preemptively activated with LPS, as an inflammatory trigger. Briefly, BV-2 cells were seeded in 24-well plates at a density of 1×10^5 viable cells/cm^2 and left to adhere for 24 h. After 24 h, the medium was removed, and the cells were washed twice with PBS followed by the addition of 100 $ng.mL^{-1}$ of LPS for 1 h. Microglia cells were then washed again and the free drug, empty LNC, TfRp-LNC RA and TfRp-SPION-LNC RA were added in different concentrations to the cells and incubated for 4 h. After 4 h, the supernatant of the cells was collected and analyzed by ELISA for the presence of interleukin-6 (IL-6), interleukin-10 (IL-10) and tumor necrosis factor-alpha (TNF-α).

2.9. Effect of lipid nanocapsules on the production of intracellular nitric oxide

Nitrites, stable metabolites of nitric oxide (NO), were assessed in the microglial cell line BV-2 after 1 h of LPS stimulation to verify the potential of the LNC to revert the production of NO. Nitrites were dosed using the Griess assay as previously described. Briefly, cells were plated in a 24-multiwell plate at density of 2.5×10^4 viable cells/cm^2 and were exposed to LPS at concentration of 100 $ng.mL^{-1}$ for 1 h. Afterwards, cells were incubated with empty LNC, RA, TfRp-LNC RA and TfRp-SPION-LNC RA for another 4 h. Lastly, the supernatants were incubated into a 96-well plate with an equal volume of Griess reagent. The absorbance was measured at a wavelength of 550 nm after 1 h of incubation at RT using a fluorescent microplate reader (BioTeK® Synergy MX, Winnoski, VT, USA).

2.10. Oligodendrocyte-progenitor cell immunocytochemistry and image acquisition

OPCs were seeded in a 24-well plate at a density of 3.1×10^4 viable cells/cm^2. After 24 h for cellular adhesion, the medium was removed and the cells were incubated with LNC, RA, TfRp-LNC RA and TfRp-SPION-LNC RA. After 4 h, the medium with the LNC was removed again and fresh medium was added. At day 2 and 5 of differentiation, the cells were fixed following the same procedure described in 2.6, for 15 min and further permeabilized and blocked in PBS containing 5% (*v*/v) normal donkey serum (NDS) and 0.3% (v/v) Triton X-100. Primary antibodies were diluted in PBS containing 1% (v/v) NDS and 0.15% (v/v) Triton X-100 and incubated overnight in a humid chamber at 4 °C. The following primary antibodies were used: rabbit anti-Olig2 (1:400), rat anti-MBP (1:100) and mouse anti-alpha tubulin (1:2000). Secondary antibodies Alexa-Fluor 488, 568 and 647 were applied for 1 h at RT and subsequently treated for nuclear counterstaining at RT with Hoechst at 2 $\mu L.mL^{-1}$. Qualitative images of the OPCs were obtained using a laser scanning confocal microscope (Leica SP5, 405 nm for Hoescht, 488 nm for Olig2, 568 nm for MBP and 647 nm for tubulin).

OPCs were imaged using the automated widefield microscope INCell Analyzer 2000 (Cytiva), with a 20× objective (N.A 0.45). 49 equally spaced fields were acquired in a 2D mode with 2 × 2 binning. Images were segmented using ilastik (version 1.3.3, https://www.ilastik. org/), followed by further segmentation and analysis using CellProfiler (version 3.1.9, https://cellprofiler.org). Final results were analyzed using Microsoft Excel (Microsoft Office 365). Outputs include the number of MBP and Olig2 positive cells, the area occupied by MBP, and the differentiation stages of oligodendrocytes based on tubulin markers. For the oligodendrocyte differentiation stages classification a method developed by Bouçanova et al. was adapted [33]. Briefly, an area around the nucleus was created and termed "collar". Only Olig2 and well-segmented cells (area of nucleus defined between 60 and 192 μm^2 and area of the collar defined between 720 and 1000 μm^2) were considered for the analysis. The area of the tubulin protrusions was measured inside the collar area and the percentage of occupancy was related with the oligodendrocyte stage. Cells in stage I were classified as having <20% of occupancy area, in stage II between 21 and 32%, stage II between 33 and 51% and finally, stage IV cells >52%.

For the analysis of the MBP and the Olig2 positive cells, classification was performed using CellProfiler Analyst (version 2.2.1, https://cellprofiler.org/cp-analyst/), through the Random Forest algorithm, with user-defined classes. At least 100 objects were included in each class, to create a complete training set and to ensure reliable outcomes. Once the accuracy of classification was above 90%, the classifier was used for batch processing and the cells were staged using Microsoft Excel.

2.11. Statistical analysis

For the performed statistical and data analysis, the software GraphPad Prism Version 9.0.1 was used. To verify the differences between groups, one-way or two-way analysis of variance (ANOVA) were applied. Normality was verified by the Shapiro-Wilk and Kolmogorov-Smirnov test. In case of no normality, a logarithmic transformation was applied, and the results analyzed by one-way ANOVA. Differences between groups were compared with a *post hoc* test (Tukey's honestly significant difference). Results are reported as mean ± standard deviation (SD) from a minimum of three independent experiments. Differences were considered significant at $*p < 0.05$, $**p < 0.01$, $***p < 0.001$ or $****p < 0.0001$.

3. Results and discussion

3.1. TfRp-SPION-LNC RA production and characterization

TfRp-SPION-LNC RA were proposed to improve the targeting

potential to the brain and to maximize the therapeutic effectiveness of compounds towards the CNS in demyelinating conditions. The SPION-LNC RA were developed by a phase-inversion methodology as previously described [10]. To promote the covalent link between the cysteine amino acid of the TfR-binding peptide and the surface of the LNCs, the shell of the LNCs was modified to present a functional group - maleimide was chosen because of the ease of reaction with the thiol entity of the cysteine amino acid of the TfR-binding peptide [34].

The physico-chemical characterization of the TfRp-LNCs showed that the developed nanosystem presented an average size of around 100 nm, a monodisperse size distribution (average PdI of around 0.2), and a slightly negative zeta-potential. To achieve this size, the ratio of the excipients respected a previously determined balance [35]. Previous studies have showed that particles of around 100 nm have an improved interaction with the targeted receptors at the surface of BBB cells, and even in some cases passive diffusion through the BBB tight junctions [36–38]. Across all the formulations, for a theoretical drug loading in mg of RA per grams of lipids of 2.28 mg.g^{-1} of RA, high encapsulation (over 88%) of RA was always accomplished due to the innate affinity of RA to the oily lipids present at the core of the LNC. Interestingly, when the process was scaled-up, the association efficiency was even higher, with practically all RA being encapsulated. This is likely due to the higher quantities of available lipids to react with the RA ensuring a more efficient encapsulation process. The theoretical loading can also be increased by several fold for LNC, although in our case it was not necessary due to the minute doses necessary for RA to have an action.

The modification of the LNCs with the TfR-binding peptide resulted in a significant increase in the size of the LNCs (from 77 nm to 109 nm, respectively) and made them more heterogeneous regarding size distribution (0.134 to 0.299 PdI, respectively). This phenomenon was already reported as a consequence of the process of surface functionalization *per se* [39]. Despite this, the TfRp functionalization did not affect the preservation of the payload of the LNCs. The functionalization process was verified by the presence of elementar Sulphur on the final formulation compared to the absence of it in unfunctionalized batches by elemental dispersive scanning (Table S1). The SPIONs, were quantified by the *ortho*-phenanthroline, and it was found that by the direct method of destroying the LNC by the same method used to quantify RA, only around 50% was detected (Table 1). The incorporation within the matrix of the LNC however was verified by TEM microscopy (Fig. 1) where the SPIONs can be seen within the matrix of the LNC. However, it should be noted that it was not feasible to separate the SPIONs from the destroyed LNC so it is not possible to assess that the association efficiency represents the total incorporation of the quantified SPIONs, and some might be deposited around the shell of the LNC. The functionalization process did not affect the incorporation of the SPIONs within the formulation, which had identical association efficiency values.

Table 1
Physico-chemical properties of the different formulations of RA-loaded and unloaded LNC. Results from $n = 3$ independent experiments, Mean +/− SD. *$p < 0.05$, compared to the empty LNC.

Formulation	Size (nm)	PdI	Zeta-potential (mV)	RA association efficiency (%)	SPION association efficiency (%)
Empty-LNC	77 ± 1	0.134 ± 0.006	−3.51 ± 0.67	–	–
LNC RA	70 ± 3	0.130 ± 0.020	−3.69 ± 1.01	90.6 ± 3.1	–
SPION-LNC RA	78 ± 1	0.126 ± 0.018	−8.34 ± 1.65	87.6 ± 2.8	53.5 ± 0.5
TfRp-SPION-LNC RA	109 ± 12*	0.299 ± 0.034	−7.21 ± 0.80	87.6 ± 2.8	53.5 ± 0.5
LNC RA (10×)	68 ± 1	0.081 ± 0.017	−5.94 ± 0.58	98.4 ± 0.5	–
SPION-LNC DiD	74 ± 0	0.200 ± 0.010	−2.73 ± 0.20	–	53.5 ± 0.5

The characteristics of the different formulations are presented in Table 1.

TEM and cryo-SEM imaging were performed to observe the LNC morphology, and to understand their overall organization and structure (Fig. 1). The images showed a size-uniform population that is in accordance with the observed PdI (Table 1). Due to the small size of the LNC, the cryo-SEM images appeared to have some mild deformation. This is due to the intensity of the electron beam on the LNC due to their smaller size, bordering on the resolution limit of the cryo-SEM.

To confirm that the LNC were able to preserve RA and were ideal candidates for long-term storage at 4 °C, their physico-chemical properties were assessed every 3 months (Table S2). After 9 months of storage, the LNC were able to preserve their size around 70 nm, PdI of 0.1 and around 90% encapsulation efficiency of RA without premature degradation. This was verified only for unfunctionalized LNC, as the functionalization process was always done previous to any assay.

The release profile of RA from TfRp-SPION-LNC RA was also verified and compared with the diffusion profile of free RA through the dialysis membrane. Through 8 days, the release profile was found to be <1% in simulated biological media (Fig. S1). This is in accordance with previously reported release profiles of LNC as they tend to have sustained release due to their innate stability, and only release their payload after fusion with the cell membranes [40].

Fluorescently labeled LNC encapsulating DiD instead of RA were developed to be used in assays were live fluorescent tracking of the LNC was required. Anthocyanin dyes have been used in lipidic nanosystems [41] due to their ease of encapsulation and overall stability without premature release of the system [42]. The physico-chemical properties of LNC incorporating DiD were identical to LNC encapsulating RA (Table 1), meaning that these are ideal candidates to mimic the properties of the properties of these in imaging assays.

3.2. *In vitro nanocapsule safety and cell interaction*

3.2.1. *Effect of lipid nanocapsules on cell metabolic activity*

One of the main obstacles to the use of LNC for brain delivery is their innate cytotoxicity. Specifically, the high concentrations of lipids and surfactants at the surface of LNC make them noticeably toxic for cells, thus special considerations should be accounted for when designing LNC based nanosystems. As LNC normally hold high encapsulation efficiencies of lipid drugs, this issue can be avoided by promoting higher dilutions to reduce the lipid content to tolerable levels. Here the cytotoxicity of the developed LNC formulations was studied after 4 h and 24 h of exposition on hCMEC/D3 brain endothelial cells, BV-2 microglia cells and primary rat OPCs. The MTT and resazurin assays were chosen to infer the cytotoxicity profiles from cellular metabolic changes. A range of concentrations was chosen, that was selected based on the quantity of lipids of the LNC (5.5 mg.mL^{-1}, 11 mg.mL^{-1} and 22 mg.mL^{-1}), and expressed in its equivalent concentration of RA (1 μg.mL^{-1}, 2 μg.mL^{-1} amd 4 μg.mL^{-1}, respectively) for the empty LNC, TfRp-LNC RA and the free RA. The concentrations were based on the range of concentrations wherein RA was shown to have an impact on the promotion of differentiation of neural stem cells of the CNS and suppress activated microglia [2,43].

On hCMEC/D3 cells it was noticeable some toxicity at 4 h for the highest concentrations, although still above the 70% threshold for all the LNC formulations (Fig. 2). At 24 h, the toxicity at higher concentrations is severe, even for free RA, but at the lowest concentration the LNC and RA were still well tolerated. It is worth noting that the results were similar to reported values in the literature. In one study, LNC decorated

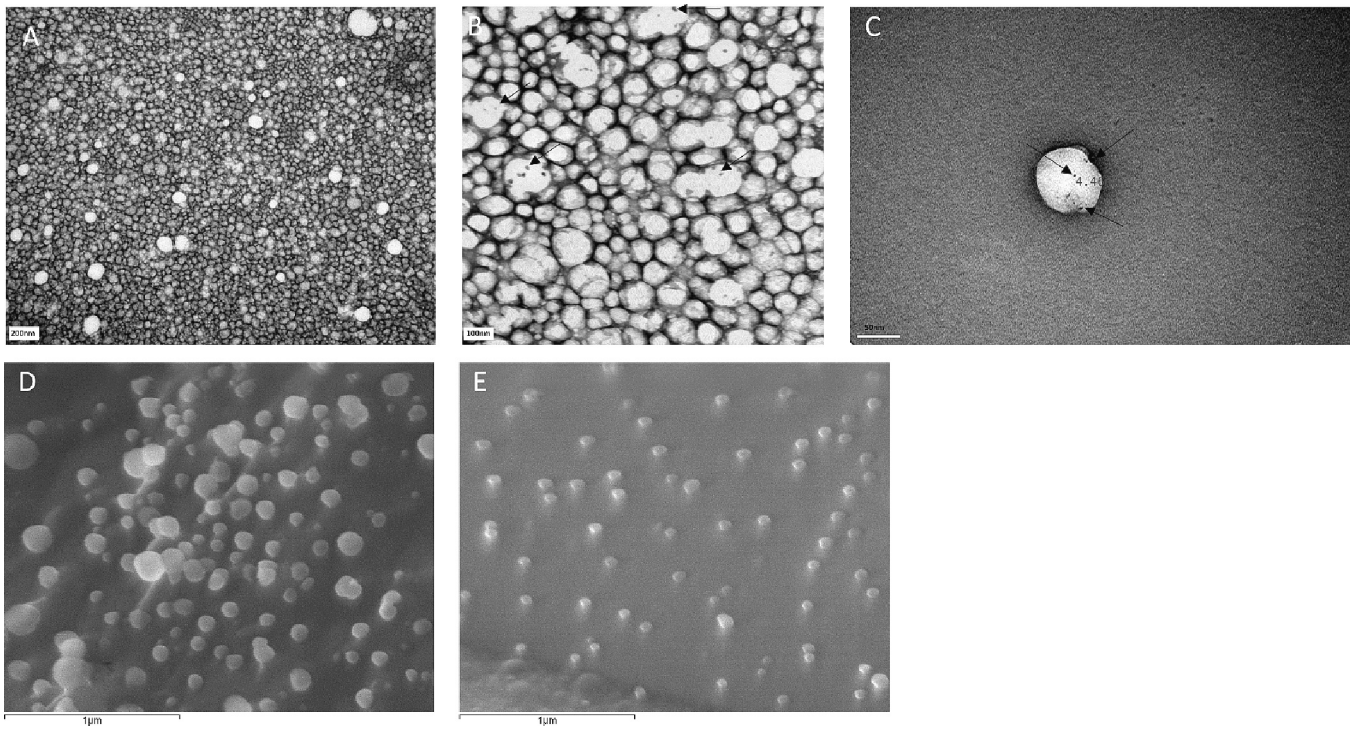

Fig. 1. TEM (Top) and cryo-SEM (bottom) of SPION-LNC RA. (A) 50,000× magnification, scale bar corresponding to 200 nm, (B) 100,000× magnification, scale bar corresponding to 100 nm, black arrows indicate SPIONs within the matrix of the LNC, (C) is an image of an individualized LNC showcasing the SPIONs (black arrows) within and the size measurement corresponding to the defined size of the SPIONs (5 nm), scale bar corresponding to 50 nm. (D) and (E) cryo-SEM of two different fields, scale bar corresponding to 1 µm.

with cannabidiol were tested on hCMEC/D3 cells and it was found that, at an equivalent lipid concentration, the LNCs were tolerated above the 70% threshold [41]. It should be highlighted, however, that different excipient quantities were used between studies, thus, a straightforward comparison cannot be established. Regarding BV-2, the most notable result was the toxicity experienced at 4 h by LNC RA, that was not seen in the unloaded control. Herein, this could be due to a synergistic effect of the toxicity of the LNC and the RA at higher concentrations, as RA is known to suppress activated microglia [44]. At 24 h, similarly to hCMEC/D3, marked toxicity was observed at higher concentrations with LNC, but also significant toxicity of the higher concentrations of RA. Paradoxically, one study tested polymeric nanoparticles with RA at higher equivalent concentrations of RA, although on a different microglial cell line [45]. The study, however, did not show the marked toxicity exhibited in our results, perhaps symbolizing a potential different response of microglial cell lines to the presence of RA. With the results herein presented of cell metabolic activity assays, the concentration of 1 $\mu g.mL^{-1}$ was considered as the threshold for the following assays.

However, when the OPCs were assayed on the same concentrations at hCMEC/D3 and BV-2, it was found that at the higher timepoint (24 h) and the same concentrations as the other cells, complete toxicity was observed (data not shown). Thus, as the primary cells were more sensitive to the action of the LNC, for any assay regarding the OPCs, lower concentrations and timepoints were used (Fig. 2). The LNC were well tolerated at selected concentrations (0.055 $mg.mL^{-1}$ amd 0.5 $mg.mL^{-1}$ equivalent in lipids, corresponding to 0.01 $\mu g.mL^{-1}$ and 0.1 $\mu g.mL^{-1}$ RA, respectively) and time point (4 h of incubation). These results are in line with previously reported works in the literature, where LNC at equivalent surface lipid concentrations was incubated for 1 h with OPC and showed no toxicity after 1 and 7 days [27]. Another work demonstrated that a nose-to-brain delivery route of LNC encapsulating the anti-inflammatory bioactive lipid prostaglandin D_2-glycerol ester (PGD_2-G) in an experimental autoimmune encephalomyelitis model had no impact on myelinating oligodendrocytes or OPC differentiation [46].

3.2.2. *Assessment of lipid nanocapsule-cell interaction*

The cell interaction of TfRp-SPION-LNC was performed using DiD as a fluorescent marker to track the cells and it was verified by flow cytometry. Confocal microscopy was also used to allow a qualitative analysis of the interaction of the LNC with the BBB endothelia. DiD was encapsulated within the matrix of the LNC. As the fluorescent dye DiD is described as stable within the LNC core, even in lipophilic environments, the observable fluorescence is indicated to be the TfRp-SPION-LNC DiD and not the released dye [42].

The outcomes of flow cytometry were expressed through the median fluorescence intensity (MFU), as represented in Fig. 3. It is observable that the presence of TfRp at the surface of LNC improved 3- to 4-fold the cell uptake when compared to the unfunctionalized LNC, suggesting the use of the TfR pathway to internalize the LNC. Furthermore, when establishing a direct competition assay, in the presence of TfRp previously added to the media, the uptake was slightly below the functionalized LNC, but still 2-fold higher than the unfunctionalized LNC, suggesting the high affinity of the LNC to the TfR receptor. These results are in line with previously reported results regarding the functionalization of the surface of the LNC, which has already been demonstrated before as being significantly beneficial to their uptake by target cells despite the high rates of unspecific uptake due to the lipid composition of the LNCs [27,31].

To verify the results from flow cytometry, confocal microscopy analysis showed that the TfRp-SPION-LNC have an increased interaction with the cells, as compared to the unfunctionalized LNC. The localization of the internalized LNC, with a widespread distribution throughout the cell rather than membranal accumulation, which is more indicative of pinocytic uptake rather than endosomal accumulation suggests that the LNC were uptaken by receptor-mediated transcytosis [47]. To confirm that the LNC were in fact inside the cells and not deposited around the cell membrane, the orthogonal projection is presented. The results from the physico-chemical alterations, flow cytometry and confocal microscopy strongly suggest the successful functionalization of

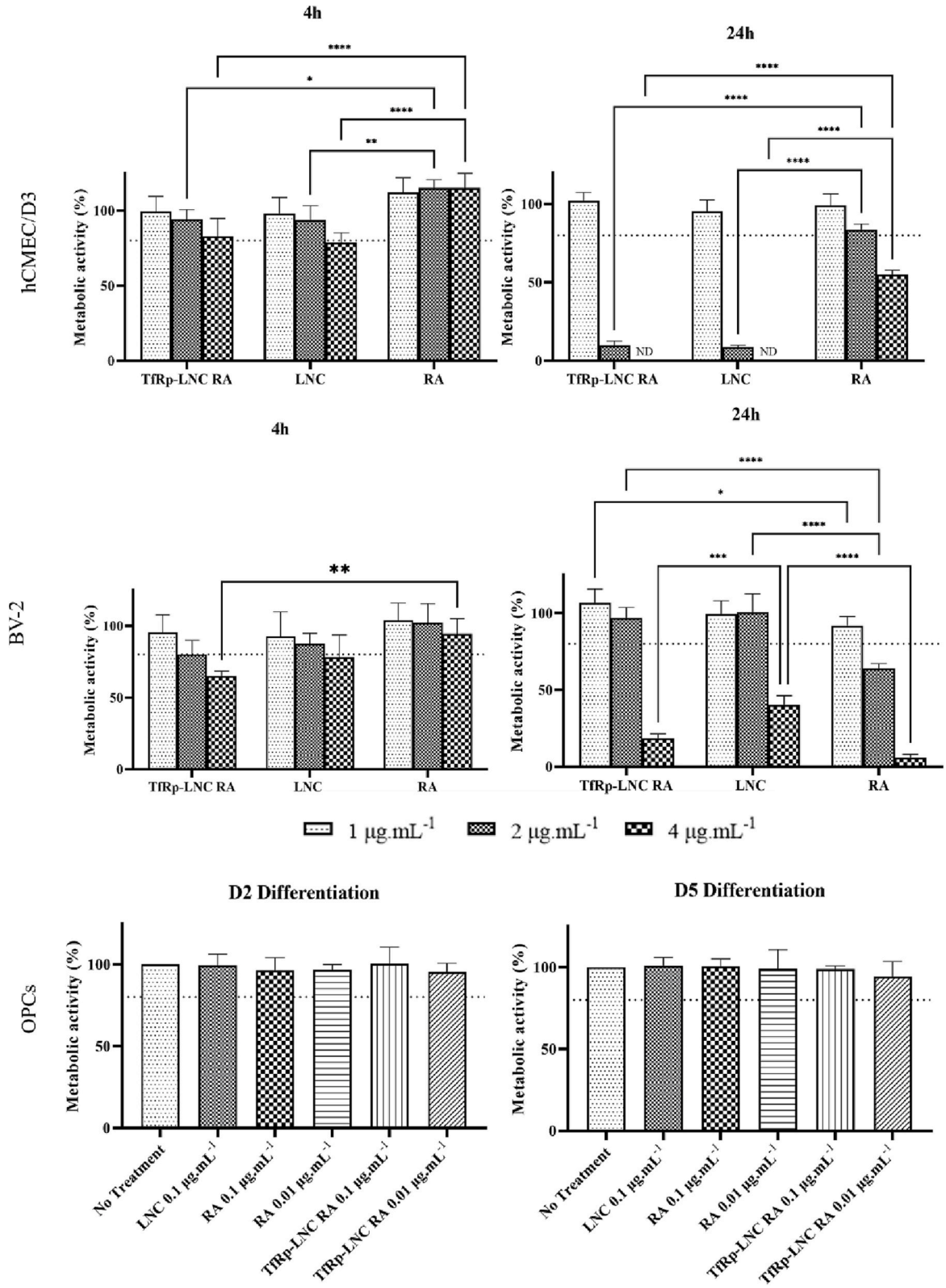

Fig. 2. Metabolic activity of brain endothelial cells (hCMEC/D3, top graphs) at 4 h and 24 h, Metabolic activity of microglia cells (BV-2, middle graphs) at 4 h and 24 h and metabolic activity of primary OPCs in the presence of empty LNC, free RA, TfRp-LNC RA for 4 h, at days 2 and 5 of differentiation. Values were normalized to the non-treated cells. The concentration of RA was calculated based upon dilution factors of LNC. Results from $n = 3$ independent experiments (three replicates per condition); Mean +/− SD *$p < 0.05$; **$p < 0.01$; ***$p < 0.005$; ****$p < 0.0001$.

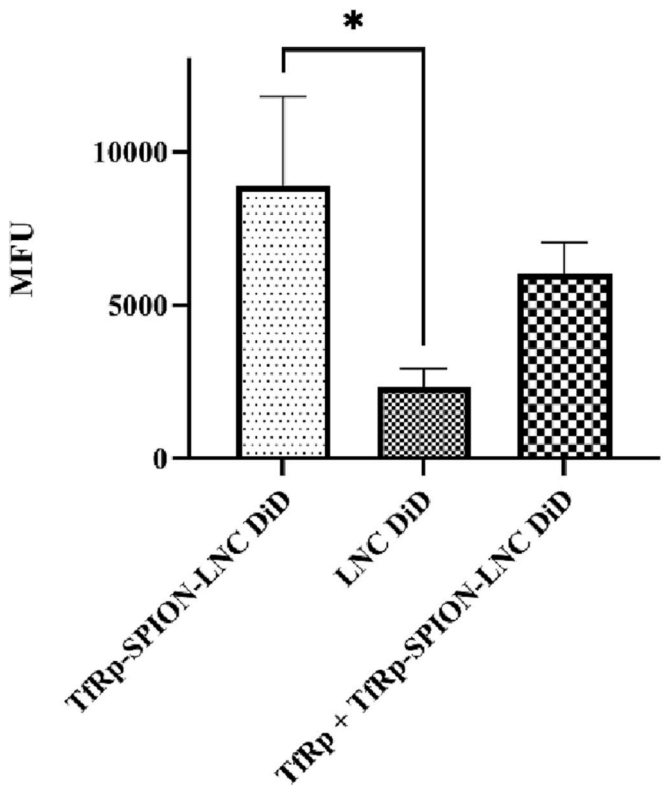

Fig. 3. Flow cytometry analysis of the *in vitro* cellular uptake of TfR-SPION-LNCs by hCMEC/D3 cells, expressed in mean fluorescence intensity (MFU). Results from $n = 3$ independent experiments, Mean +/− SD, * $p < 0.05$.

TfRp on the surface of SPION-LNC RA. We attempted to quantify the association of the peptide with the LNC by nuclear magnetic resonance (NMR) but due to the low values of peptide and the thiol bond the resolution was not able to show the chemical bond (data not shown). To further verify if the interaction between the LNC and the cells was due to TfRp and not unspecific uptake, the functionalized LNC were incubated with cells that were pre-treated with TfRp, to demonstrate a competitive assay for the receptor target. As it is visible in Fig. 4, the cells pre-treated with TfRp had noticeably less internalization than the functionalized cells without competition, suggesting that the uptake is due to the transferrin receptor. These results are in line with previous results at our group [18,48], where poly(lactic-*co*-glycolic) acid (PLGA) nanoparticles were functionalized with TfRp, in order to target the BBB in CNS disorders, and an increase in the interaction between the nanoparticles and hCMEC/D3 was verified in both studies.

The successful functionalization of a nanoparticle is critical to improve targeting to desired states and reduce the off-target effects of the drug delivery system. In this study, we have successfully demonstrated the attachment of a proven ligand that is able to guide LNCs to the BBB, which will allow controlled delivery of RA to the CNS. This is of extreme importance as the CNS is a tissue where RA was not able to reach in sufficient concentrations to have a biological effect due to poor pharmacokinetic properties.

Having this in mind, after the LNC can successfully manage the BBB, it is of paramount importance to verify their interaction with the two main target cells of the CNS within the scope of this study. As microglia are the main resident immune cells of the CNS and are usually present in neurodegenerative disorders at lesion sites in an activated site promoting the existence of an inflammatory environment. To promote the ideal conditions for the development and differentiation of OPCs into mature oligodendrocytes and result in new myelin being produce, reverting the microglia to a pro-resolutive state is a key step in ensuring the reversion of the myelin damage. Thus, it is required that the LNC can successfully interact and be internalized by microglia. The LNC demonstrated the ability to be internalized by the microglia (Fig. 5) without triggering cell apoptosis or altering their conformation towards an aggressive, scavenging, activated state. The control without treatment was performed in order to validate the impact of the LNC on microglia (Fig. S2)

The internalization of the TfRp-SPION-LNC DiD was verified at both days 2 and 5 of differentiation of OPCs, with the localization being deep within the cellular membrane of these cells (Fig. 6). The presence of the LNC in both early stage and late stage OPCs, as observable between the differing OPCs in the days 2 and 5 of differentiation, can hint towards the ability to interact early in the maturation stage of OPCs to promote improved differentiation of the OPCs towards mature, myelinating oligodendrocytes. To verify if the LNC had any impact on the OPCs, controls without LNC were performed (Fig. S3).

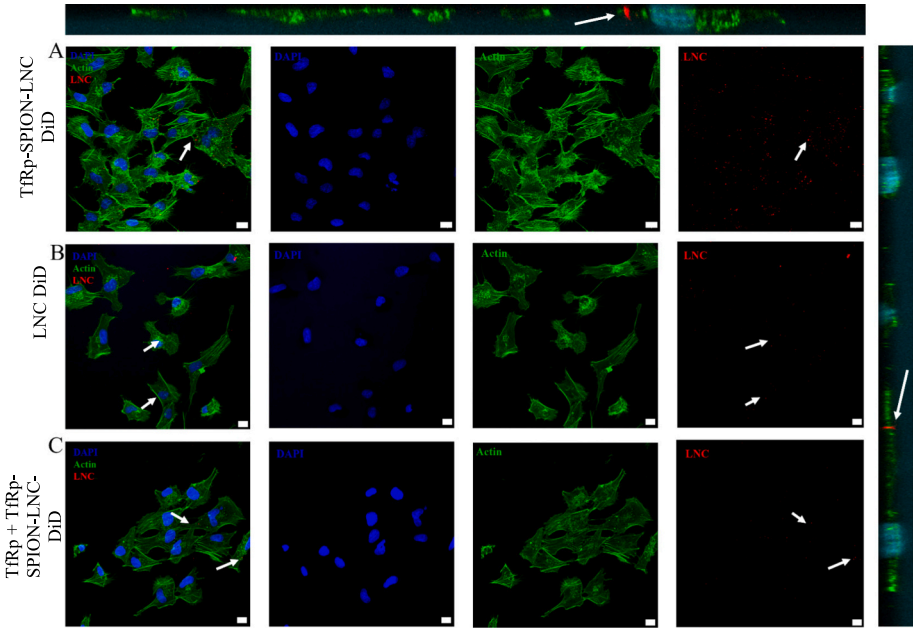

Fig. 4. Confocal fluorescence microscopy representative images of the internalization of the TfRp-SPION-LNC DiD by hCMEC/D3 cells after an incubation period of 1 h. The internalization of the LNC was significantly higher on TfRp functionalized SPION-LNC DiD (A) compared to the unfunctionalized LNC (B) and the functionalized SPION-LNC DiD with TfRp pre-treatment as a competitor assay. Top side and right side are the orthogonal projection of TfRp-SPION-LNC DiD (A) showing the internalized LNC, the arrows indicate the signal from the LNC within the membrane of the cells. The localization of the TfRp-SPION-LNC DiD, both deep within the cells' cytoplasm and on the outskirts of the membrane is a good indicator of specific interaction with the cells. Scale bar = 10 μm.

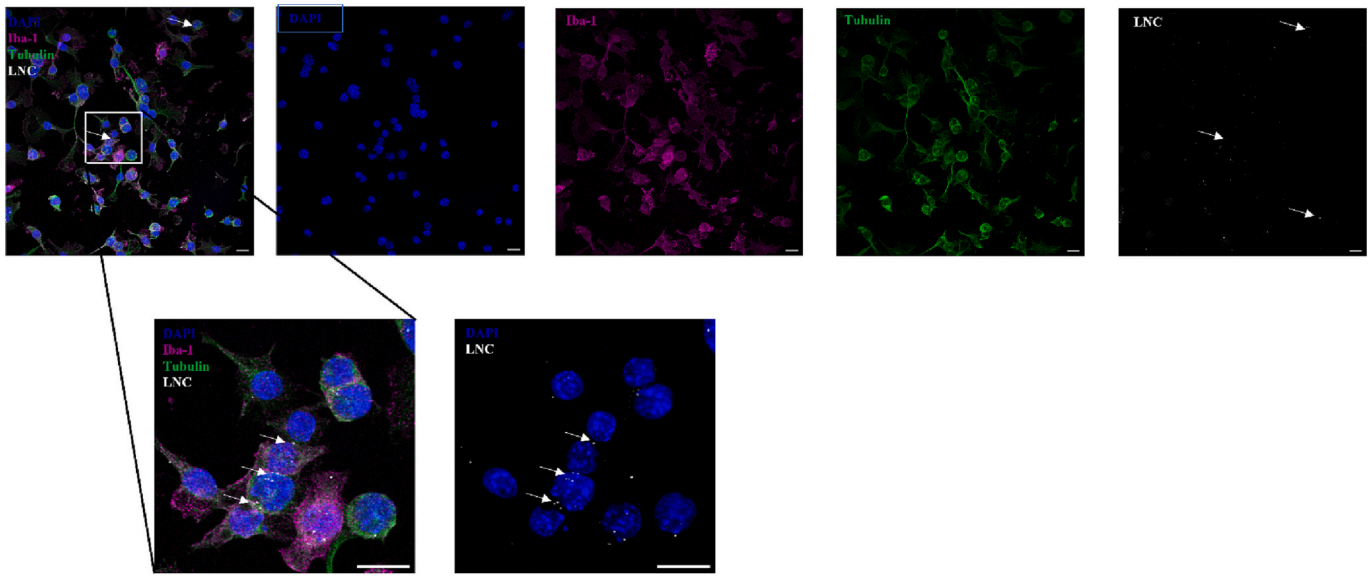

Fig. 5. Confocal fluorescence microscopy of the internalization TfRp-SPION-LNC DiD by microglia (BV-2) after an incubation period of 4 h. The LNC was found to be located deep within the microglia, and to not promote their alteration towards an ameboid state, suggesting that it does not trigger microglial activation. The arrows indicate the presence of the TfRp-SPION-LNC DiD. Magenta: Iba-1, Green: Tubulin, Blue: Hoescht. Scale bar = 20 μm. (For interpretation of the references to colour in this figure legend, the reader is referred to the web version of this article.)

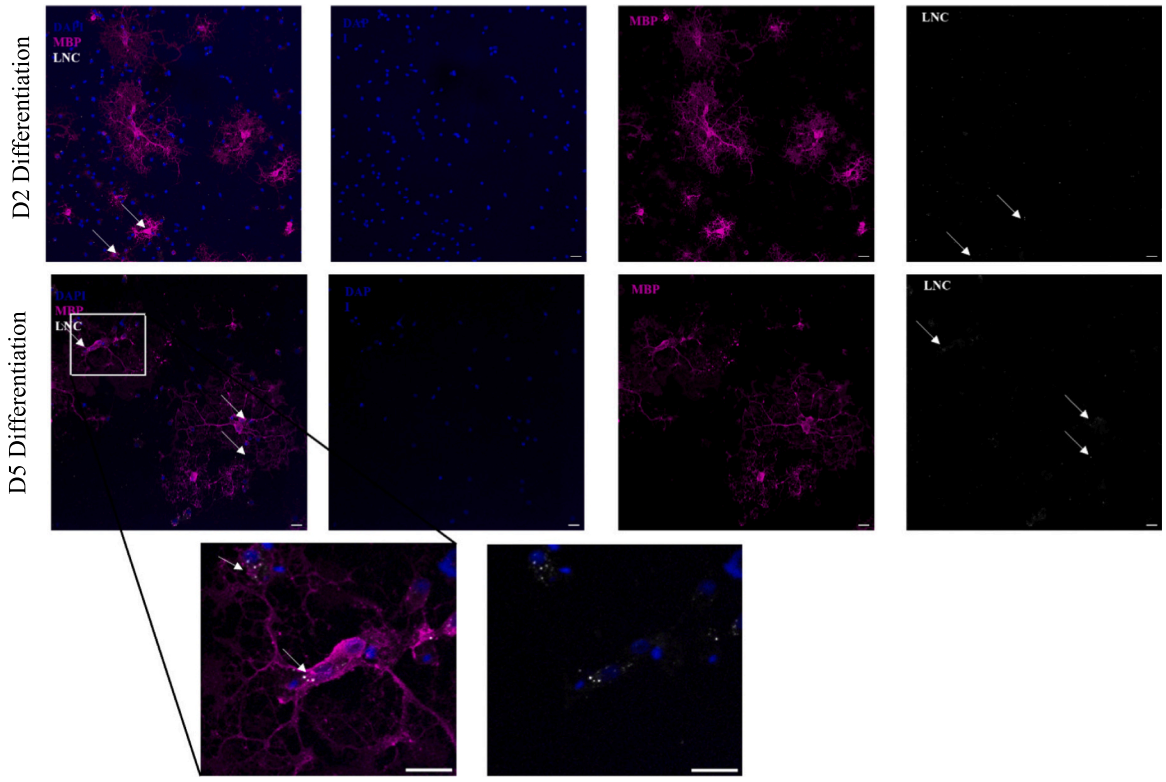

Fig. 6. Confocal fluorescence microscopy of the internalization TfRp-SPION-LNC DiD by OPCs after an incubation period of 4 h. Day 2 has OPCs with a lower degree of differentiation, already with LNC inside, while day 5 has late stage OPCs, with LNC placed close to the cell nucleus, indicating the LNC involvement from an early stage. The arrows indicate the presence of the TfRp-SPION-LNC DiD. Magenta: MBP, Blue: Hoescht. Scale bar = 20 μm. (For interpretation of the references to colour in this figure legend, the reader is referred to the web version of this article.)

3.2.3. Permeability of the lipid nanocapsules across a blood-brain barrier monolayer

To understand if LNC nanoparticles were able to permeate the physiological barrier that is the BBB, a well-established *in vitro* model of the BBB was reproduced [16]. This model based on a hCMEC/D3 cell line has several advantages over other BBB *in vitro* models, including the i) maintenance of BBB-specific properties over passages; ii) simple to maintain and low cost to reproduce; and iii) the capacity of forming functional barriers with key tight junction proteins [49].

In order to verify the potential for receptor-mediated transcytosis of

TfRp-SPION-LNC RA, the concentrations with the best results were used on the uptake and the viability assays (0.1 and 1 μg.mL^{-1} of RA), and the formulation was evaluated at 60, 120, 180 and 240 min. The permeability coefficients showed differences between conditions (Fig. 7), where the external functionalization with TfRp improved the permeability of the LNC (approximately 0% for the free drug and 3% for the functionalized LNC) after the 4 h. Throughout the assay, it was observable that all formulations experienced a linear growth in the quantities that permeated the monolayer, but the functionalized LNC demonstrated the highest values. A significant finding was the degradation observable by RA under these conditions (Table S3), wherein the encapsulation could result in some protection to ensure the cargo reaches the intracellular compartments to perform its biological activity.

These results are in line with reported applications of LNC for brain delivery, where the permeability coefficients were improved by external functionalization [41]. The improved delivery rates were also verified in other works when exploiting the transferrin pathway [16,50,51]. Having this in mind, this work suggests that this versatile platform is able improve the delivery rates of lipophilic drugs to the CNS, unlocking novel therapies that were once not feasible for administration due to poor bioavailability. The TEER remained intact throughout the assay (Fig. S4).

3.3. Anti-inflammatory and oligodendrocyte-progenitor cells differentiation potential of lipid nanocapsules

The two main events on demyelinating disease such as MS are the loss of the myelin sheath of neurons produced by oligodendrocytes and the aggressive inflammatory milieu. Microglia particularly undergoes significant activation [52], contributing to a widespread inflammatory environment in lesion sites that together with astrocytic activation eventually leads to the formation of a glial scar [53].

To understand if TfRp-SPION-LNC RA are able to hold an anti-inflammatory activity when in contact with microglia, and to decrease their activation state, BV-2 microglia cells were firstly activated by the presence of LPS for 1 h. When microglia undergo activation in response to an external stimulus, it undergoes morphological alterations that are easily observable, particularly adopting an ameboid, circular conformation rather than an elongated, branched phenotype [54]. Also, the conformation alterations are coupled with phenotypic changes, resulting in the production of pro-inflammatory cytokines. With the presence of RA after the exposure to this stimulus, the microglia can revert back to its normal conformation, drastically reducing the production of inflammatory markers and the ability to establish an inflammatory, aggressive environment [55]. To quantitatively verify if there is an actual suppression of pro-inflammatory stimuli and a shift towards an anti-inflammatory state, IL-6, TNF-α and NO were chosen as pro-inflammatory markers, and IL-10 was chosen as an anti-inflammatory indicator. The expression of these markers was quantified by ELISA (IL-6, TNF-α and IL-10) and the Greiss reaction (NO) as represented in Fig. 8. To study a potential dose-response effect, three different concentrations (0.01, 0.1 and 1 μg.mL^{-1}) were selected based upon the metabolic activity previously demonstrated in order to try to establish an active range of concentrations. Empty LNC, free RA (equivalent to the highest concentration of LNC RA, 1 μg.mL^{-1}) were used as controls to compare the anti-inflammatory action with TfRp-SPION-LNC RA on LPS stimulated cells. Non-stimulated cells were used as a negative control for the presence of anti-inflammatory biomarkers.

From the results of ELISAs and the Griess assay it is observable that RA and LNC RA have a potent anti-inflammatory action, acting on the production of NO and the cytokines IL-6, IL-10 and TNF-α. The results are in accordance with previously reported studies on the role of RA [56,57]. Here, LNC was able to preserve the activity of RA, matching up, or outperforming the free RA. All tested concentrations of RA within the LNC exhibited anti-inflammatory activity, with the highest (1 μg.mL^{-1}) exhibiting the most marked effect. This was particularly notorious on the production of the anti-inflammatory cytokine, IL-10. The concentrations of 0.01 and 0.1 μg.mL^{-1} produced 5 to 6-fold less IL-10 than 1 μg.mL^{-1} which highlighted the concentration dependent effect of RA. Interestingly, for IL-6, free RA did not have the same reduction compared to the LNC RA. This could be explained by the premature degradation of RA before it interacts with the cells, reinforcing the need for a vector to deliver this molecule. The presence of SPIONs within the LNC also did not impair the activity of RA or affected the cells in any way. The suppression of these biomarkers is in line with the mechanistic action of RA, acting through its target, the retinoid-x-receptor (RXR), and has been successfully demonstrated before as being an effective inhibitor of microglia activation [43,58]. This action occurs not only due to the effect of RA, but also its isomers, such as 9-cis-RA [58]. Our results are in accordance with these previously reported studies in the literature, suggesting that TfRp-SPION-LNC RA is a viable candidate to deliver RA to the CNS.

After demonstrating that LNC RA is able to significantly reduce the inflammatory environment, it was important to verify if it could significantly promote the differentiation of OPCs into mature, myelin producing oligodendrocytes. The differentiation stage of an oligodendrocyte represents the degree of maturity it has reached, and the higher the stage, the higher the ability to produce greater quantities of myelin [59]. Thus, to verify if LNC RA is able to improve the differentiation of OPCs we observed the expression of MBP, the main indicator for the presence of myelin, and oligodendrocyte branching based on the occupied area by the tubulin protuberances.

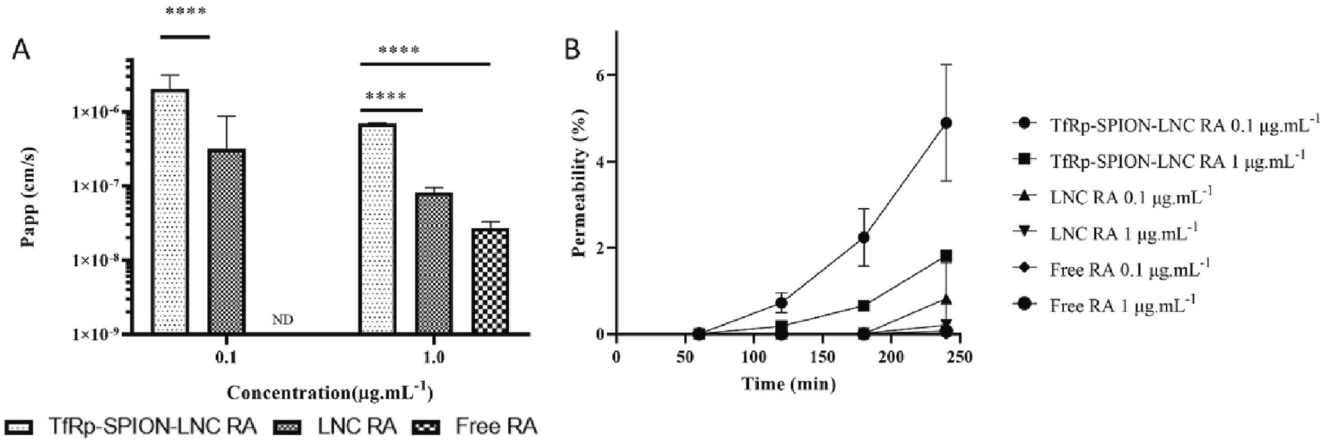

Fig. 7. Permeability of functionalized LNC compared to non-functionalized LNC and the free drug. (A) is the Papp at 4 h through a monolayer of hCMEC/D3 cells, (B) is the permeability kinetics through 4 h. Results from $N = 3$ triplicates; Mean +/− SD, ****$p < 0.0001$; ND = not detected.

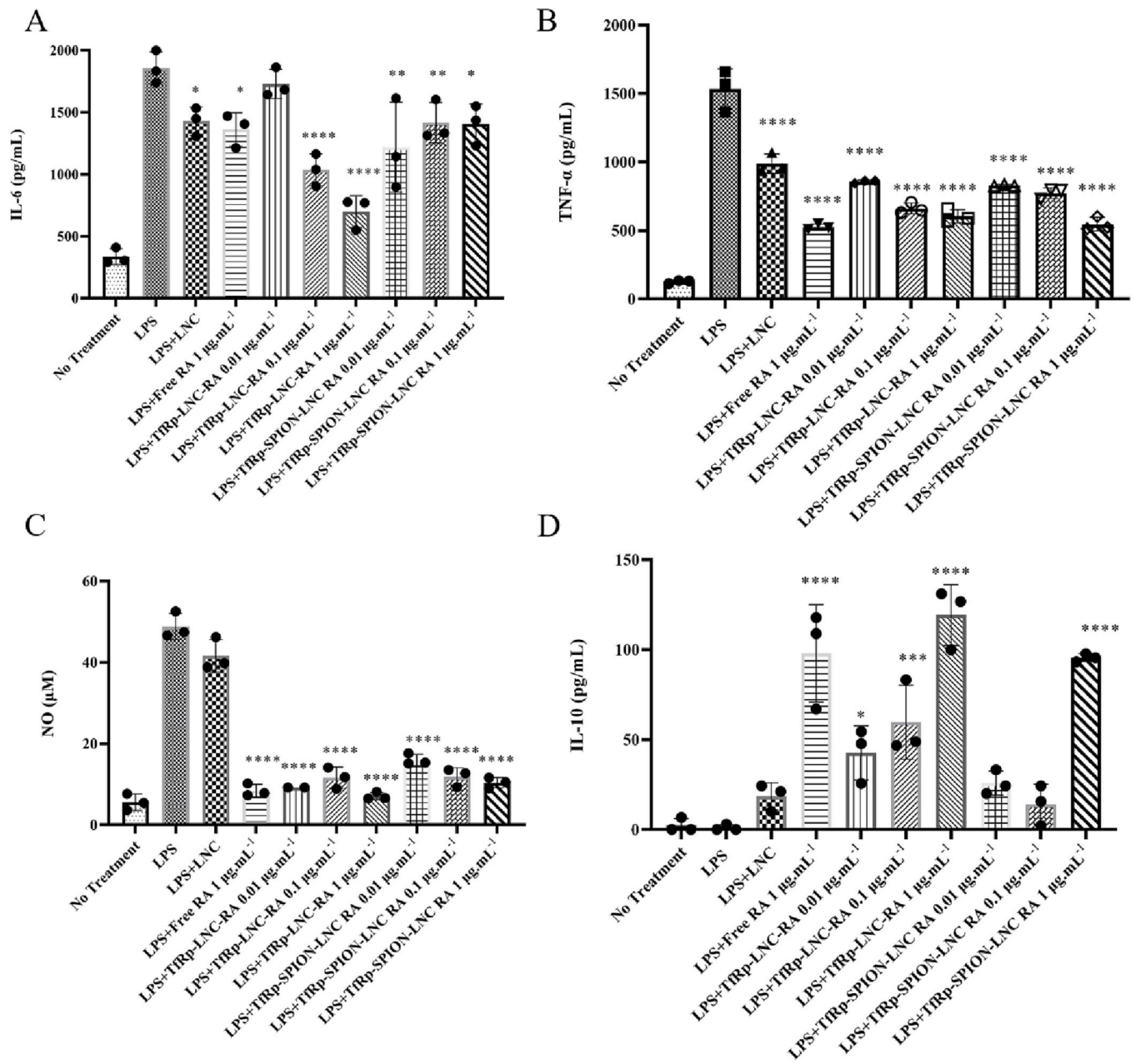

Fig. 8. Analysis of inflammatory biomarkers to verify if TfRp-SPION-LNC RA are able to establish its anti-inflammatory activity and to suppress microglia activation. A, B and C are pro-inflammatory mediators, whilst D is an anti-inflammatory cytokine, showing that RA can play both sides of the inflammatory cascade. The comparisons were always performed *versus* the LPS only well. Results from $n = 3$ independent experiments (two duplicates per condition); Mean +/− SD, $*p < 0.05$; $**p < 0.01$; $***p < 0.005$; $****p < 0.0001$.

To start, the differentiation profile of oligodendrocytes was evaluated. The impact of nanoparticles on the number of MBP cells and area occupied by each oligodendrocyte was assessed recuring to automated image analysis using open-source software. These outputs positively correlate with the ability of the cells differentiating towards a myelinating/mature state. As expected, our results show that the number of MBP positive cells increased from day 2 to day 5 of differentiation suggesting that cells are able of continuing with their intrinsic differentiation profile (Fig. 9A). Additionally, the presence of the particles did not affect the number of cells capable of producing the myelin marker MBP (Fig. 9A). Nonetheless, tendentially increased cell areas for the formulations containing RA were observed for both time-points, suggesting that the presence of RA tends to originate larger oligodendrocytes (Fig. 9B, i.-viii.).

The higher capability of RA formulations to increase oligodendrocytes' area is directly linked to the mechanism of action of RA through direct stimulation of its target receptors, notably the RXR and retinoid-A-receptor (RAR). Both receptors share similar signal transduction pathways but differ in the ligands that are able to activate them. Stimulation of these receptors has been linked particularly to improved differentiation of OPCs both *in vitro* and *in vivo* [23,60]. Particularly, direct stimulation of RXR-γ in aged rats where demyelination was induced resulted in an increase in the number of myelinated neurons, and a slight increase in MBP+ cells [61]. Another study demonstrated that mice that were knockout for the retinoid receptors experienced a delay in the recruitment of OPCs and their subsequent differentiation. Also, the mice demonstrated thinner myelin than the ones that were treated with bexarotene [62].

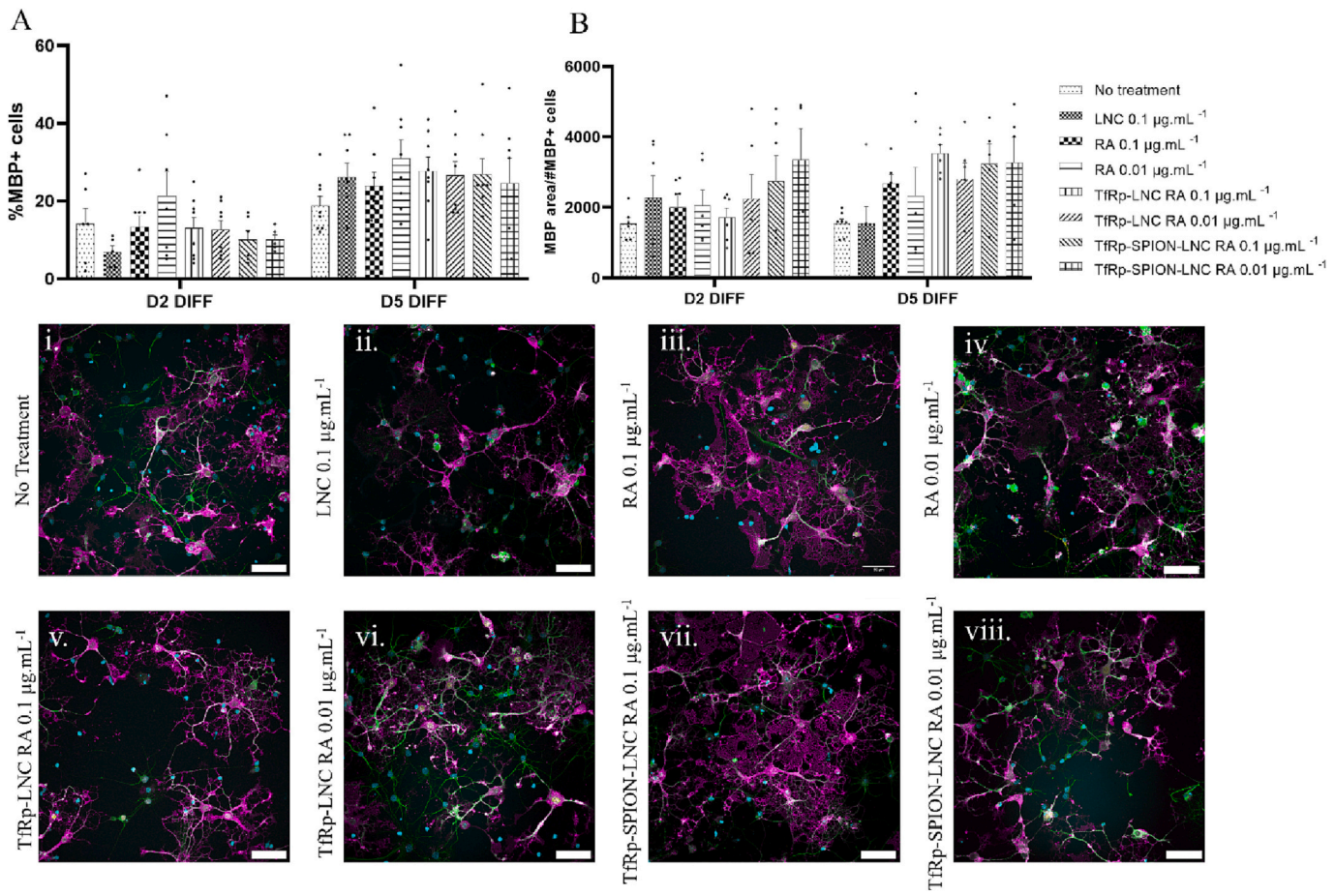

Fig. 9. MBP expression and quantification after high-throughput image screening. (A) represents the calculated expression of MBP in cells identified to be Olig2 positive (oligodendrocyte line). (B) represents the calculated ratio of the area of occupied by MBP divided by the MBP+/Olig2+ positive cells. Results are from $n = 4$ independent experiments (two replicates per condition). Data is shown as Mean +/− SD after outlier evaluation. (i-viii) Representative confocal microscopy images of each condition at day 5 of differentiation. Magenta: MBP, green: actin, yellow: Olig2, cyan: Hoechst. Scale bar = 50 µm. (For interpretation of the references to colour in this figure legend, the reader is referred to the web version of this article.)

Although our results were not able to significantly demonstrate an increase of the differentiation of OPCs, there is a significant trend implying that the presence of RA tends to improve the overall performance of OPC differentiation. These findings suggest that RA is able to affect the behavior of oligodendrocytes, promoting the development of more mature oligodendrocytes. To verify this, in order to evaluate in depth the oligodendrocyte branching ability, oligodendrocytes were categorized in four differentiation stages according to a previously established protocol ("collar occupancy") [33]. Stage I corresponds to mono- or bipolar OPCs; in stage II OPCs are primary branched with three or four processes; in stage III are secondary branched with 4–5 main processes; and stage IV corresponds to fully mature, extensively branched oligodendrocytes with membranous processes (Fig. 10 i-iv.). By estimating the area of the tubulin staining (which corresponds to protrusions of the oligodendrocytes) occupying a defined area around the nucleus ("collar occupancy") a direct relation can be established with the differentiation stage of the oligodendrocytes [33]. Here, the presence of RA, whether encapsulated within the LNC or in the free form, led to a distinct increase of late-stage oligodendrocytes at day 5 of differentiation, suggesting the ability of RA to guide the differentiation of oligodendrocytes towards their later stages of differentiation, which in due time will result in improved myelin replenishment in lesion sites. This also could point towards the potential for the LNC to promote the internalization of RA to interact with its nuclear receptors before it can be degraded. Moreover, these results are in line with previously reported results regarding the role of RA on the differentiation of OPCs [63]. It was shown that synthetic agonists of the RA receptors (RARβ and RARα) improved myelination and differentiation of oligodendrocytes in $NG2^+$ cells [60]. However, it should be noted that this study also highlighted that prolonged treatment with RA may begin to induce the upregulation of specific genes that may hinder OPC differentiation [64]. Thus, when designing a treatment focused upon RA for the differentiation of OPC the course of the treatment should be warranted to avoid a negative effect from long-term treatment.

The use of LNC has already been established and demonstrated as effective carriers to interact with OPCs, both *in vitro* and *in vivo* [2,27]. Particularly, *in vivo* LNC demonstrated the ability to restore the percentage of mature oligodendrocytes to pre-lesion levels in a mice model of focal demyelination through a stereotaxic injection 7 days post treatment [2]. Despite this, not many nanotechnology-based approaches to target OPCs have been used in the literature. A work compared the effectiveness of liposomes to polymeric particles to extracellular vesicles, and it demonstrated that despite lower uptake values, extracellular vesicles showed the best ability to induce OPCs differentiation. As LNC more closely resemble a carrier vesicle, but also benefit from some of the properties of liposomes and polymeric nanoparticles, such as better cargo loading and stability, as well as the use of biocompatible excipients, they could prove to be an efficient carrier to target OPCs [65]. Despite this, there is still a critical necessity to improve the studies and the overall study design in approaches to target OPCs to attempt to develop an optimal system to tackle demyelinating pathologies.

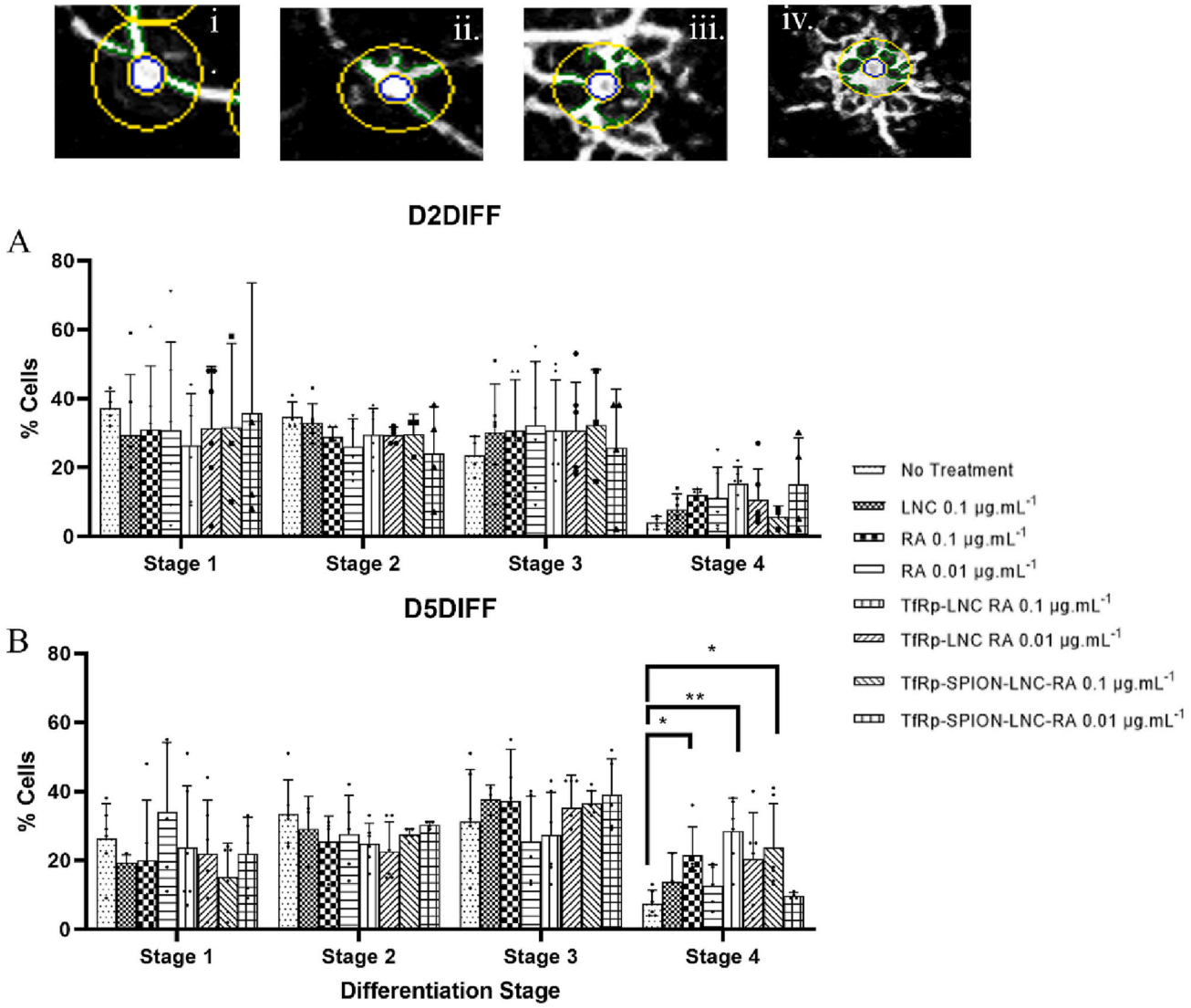

Fig. 10. Collar Occupancy analysis of the differentiation stages of OPCs. (A) are the results from the 2nd day of differentiation, while (B) is the results from the 5th day of differentiation. The cells are classified on their stages based on the area that the protrusions from the nuclei occupies relating to the area of the nuclei, as demonstrated on images (C—F). (C) is stage I; (D) is stage II; (E) is stage III; and (F) is stage IV. Results are from $n = 3$ independent experiments (two duplicates per condition). $^{*}p < 0.05$; $^{**}p < 0.01$.

4. Conclusions

In this work, a BBB-targeted LNC-based nanosystem was developed and its impact on the metabolic activity and interaction of target cells evaluated, as well as on disease associated relevant parameters, aimed at tackling MS. Particularly, monodisperse LNCs were developed, and surface functionalized with the addition of TfRp. The aim of this strategy to promote active brain targeting resulted in a 3-fold increase in the uptake by BBB endothelial cells, which can be further potentiated by the coupling with the encapsulation of SPIONs for the potential magnetic targeting in *in vivo* models. This is a candidate strategy that can be translated to other types of LNCs that could significantly improve brain delivery of therapeutics. The LNCs demonstrated a dose-dependent cytotoxicity when in contact with microglia and endothelial cells with a safe concentration range of around 1 $\mu g.mL^{-1}$ of encapsulated RA. We successfully demonstrated that encapsulation within the functionalized LNC resulted in significant improvement of the permeability profile of RA through the BBB and demonstrated that the LNC are able to be internalized by endothelial cells, microglia and OPCs in order to exert its action. Following that, the LNC demonstrated the ability to preserve the bioactive role of RA when in contact with microglia, resulting in suppression of three different pro-inflammatory cytokines by 5–6-fold compared to no treatment at all and a 100-fold improvement on the production of the anti-inflammatory cytokine IL-10 was also demonstrated. Regarding the OPCs, the LNC were able to significantly improve by 2–3-fold the presence of late stage, mature oligodendrocytes that are more capable of producing higher quantities of myelin, and demonstrated improved performance when compared to the free RA. There was also a noticeable trend on the amount of MBP+ cells and the area occupied by them when RA was present in the formulation. The particular significance of this results is because RA lacks the ability to reach the brain in significant concentrations due to premature degradation and a necessity of a specific carrier protein to circulate in the bloodstream. Thus, the TfRp-functionalized LNCs coupled with the SPIONs nonetheless act as a versatile carrier that could encapsulate other types of lipidic drugs that could be used to achieve higher concentrations at the CNS, in the scope of neurodegenerative diseases. Further work should be carried out now to validate the nanosystem *in vivo*, to confirm the improved targetability towards the brain by the co-encapsulation of SPIONs, and to establish a proof-of-concept in a

demyelinating disorder model.

CRediT authorship contribution statement

Rui Pedro Moura: Conceptualization, Methodology, Validation, Investigation, Writing – original draft, Formal analysis, Visualization. **Eva Daniela Carvalho:** Conceptualization, Methodology, Data curation, Writing – review & editing. **Cláudia Martins:** Conceptualization, Writing – review & editing. **Anne des Rieux:** Conceptualization, Writing – review & editing, Supervision. **Ana Paula Pêgo:** Conceptualization, Writing – review & editing, Supervision, Funding acquisition, Resources. **Bruno Sarmento:** Conceptualization, Validation, Resources, Writing – review & editing, Supervision, Project administration, Funding acquisition.

Data availability

Data will be made available on request.

Acknowledgements

Rui Pedro Moura, Eva D. Carvalho and Cláudia Martins thank Fundação para a Ciência e a Tecnologia (FCT), Portugal for financial support (Grant SFRH/BD/143196/2019, SFRH/BD/140363/2018 and SFRH/BD/137946/2018, respectively). Ana P. Pêgo and Eva D. Carvalho acknowledge the funding from Air Force Defense Research Sciences Program, USA (Award FA9550-20-1-0417). This project has received funding from the European Union's Horizon 2020 research and innovation programme under grant agreement No 951723. The authors acknowledge the support of the i3S Scientific Platforms Bioimaging and Histology and Electron Microscopy (HEMS), members of the national infrastructure PPBI–Portuguese Platform of Bioimaging (PPBI-POCI-01-0145-FEDER-022122). The authors acknowledge the crucial assistance of Emilia Cardoso with flow cytometry experiments, and Maria Lázaro with confocal microscopy experiments. The authors also acknowledge the support of the Biointerfaces and Nanotechnology, Translational Cytometry and BioSciences Screening i3S Scientific Platforms. The authors also acknowledge the support of the Centro de Materiais da Universidade do Porto (CEMUP), particularly Daniela Silva for cryo-SEM analysis and Sílvia Maia for LC/MS analysis.

Appendix A. Supplementary data

Supplementary data to this article can be found online at https://doi.org/10.1016/j.jconrel.2023.04.034.

References

[1] R. Dobson, G. Giovannoni, Multiple sclerosis - a review, Eur. J. Neurol. 26 (2019) 27–40.
[2] D. Carradori, Y. Labrak, V.E. Miron, P. Saulnier, J. Eyer, V. Préat, A. des Rieux, Retinoic acid-loaded NFL-lipid nanocapsules promote oligodendrogenesis in focal white matter lesion, Biomaterials 230 (2020), 119653.
[3] U. Fünfschilling, L.M. Supplie, D. Mahad, S. Boretius, A.S. Saab, J. Edgar, B. G. Brinkmann, C.M. Kassmann, I.D. Tzvetanova, W. Möbius, F. Diaz, D. Meijer, U. Suter, B. Hamprecht, M.W. Sereda, C.T. Moraes, J. Frahm, S. Goebbels, K.-A. Nave, Glycolytic oligodendrocytes maintain myelin and long-term axonal integrity, Nature 485 (2012) 517–521.
[4] N. Ghasemi, S. Razavi, E. Nikzad, Multiple sclerosis: pathogenesis, symptoms, diagnoses and cell-based therapy, Cell J. 19 (2017) 1–10.
[5] E.D. Carvalho, M.R.G. Morais, H.P. Ferreira, M.M.C. Silva, S.C. Guimarães, A. P. Pêgo, A paradigm shift: bioengineering meets mechanobiology towards overcoming remyelination failure, Biomaterials 283 (2022), 121427.
[6] B. Ettle, J.C.M. Schlachetzki, J. Winkler, Oligodendroglia and myelin in neurodegenerative diseases: more than just bystanders? Mol. Neurobiol. 53 (2016) 3046–3062.
[7] S.B. Claflin, S. Broadley, B.V. Taylor, The effect of disease modifying therapies on disability progression in multiple sclerosis: a systematic overview of meta-analyses, Front. Neurol. 9 (2018) 1150.
[8] A. Abdelhak, M.S. Weber, H. Tumani, Primary progressive multiple sclerosis: putting together the puzzle, Front. Neurol. 8 (2017) 234.
[9] R.P. Moura, C. Martins, S. Pinto, F. Sousa, B. Sarmento, Blood-brain barrier receptors and transporters: an insight on their function and how to exploit them through nanotechnology, Expert Opin. Drug Deliv. 16 (2019) 271–285.
[10] B. Heurtault, P. Saulnier, B. Pech, J.-E. Proust, J.-P. Benoit, A novel phase inversion-based process for the preparation of lipid nanocarriers, Pharm. Res. 19 (2002) 875–880.
[11] R.P. Moura, C. Pacheco, A.P. Pêgo, A. des Rieux, B. Sarmento, Lipid nanocapsules to enhance drug bioavailability to the central nervous system, J. Control. Release 322 (2020) 390–400.
[12] N.T. Huynh, C. Passirani, P. Saulnier, J.P. Benoit, Lipid nanocapsules: a new platform for nanomedicine, Int. J. Pharm. 379 (2009) 201–209.
[13] L.A. Fiel, R.V. Contri, J.F. Bica, F. Figueiró, A.M. Battastini, S.S. Guterres, A. R. Pohlmann, Labeling the oily core of nanocapsules and lipid-core nanocapsules with a triglyceride conjugated to a fluorescent dye as a strategy to particle tracking in biological studies, Nanoscale Res. Lett. 9 (2014) 233.
[14] S. Hirsjärvi, S. Dufort, G. Bastiat, P. Saulnier, C. Passirani, J.-L. Coll, J.-P. Benoît, Surface modification of lipid nanocapsules with polysaccharides: from physicochemical characteristics to in vivo aspects, Acta Biomater. 9 (2013) 6686–6693.
[15] W.A. Jefferies, M.R. Brandon, S.V. Hunt, A.F. Williams, K.C. Gatter, D.Y. Mason, Transferrin receptor on endothelium of brain capillaries, Nature 312 (1984) 162–163.
[16] M.J. Gomes, P.J. Kennedy, S. Martins, B. Sarmento, Delivery of siRNA silencing P-gp in peptide-functionalized nanoparticles causes efflux modulation at the blood–brain barrier, Nanomedicine 12 (2017) 1385–1399.
[17] M.D. Cayero-Otero, M.J. Gomes, C. Martins, J. Álvarez-Fuentes, M. Fernández-Arévalo, B. Sarmento, L. Martín-Banderas, In vivo biodistribution of venlafaxine-PLGA nanoparticles for brain delivery: plain vs. functionalized nanoparticles, Expert Opin. Drug Deliv. 16 (2019) 1413–1427.
[18] M.J. Gomes, C. Fernandes, S. Martins, F. Borges, B. Sarmento, Tailoring lipid and polymeric nanoparticles as siRNA carriers towards the blood-brain barrier - from targeting to safe administration, J. NeuroImmune Pharmacol. 12 (2017) 107–119.
[19] B.T. Tan, L. Wang, S. Li, Z.Y. Long, Y.M. Wu, Y. Liu, Retinoic acid induced the differentiation of neural stem cells from embryonic spinal cord into functional neurons in vitro, Int. J. Clin. Exp. Pathol. 8 (2015) 8129–8135.
[20] B. Cassani, E.J. Villablanca, J. De Calisto, S. Wang, J.R. Mora, Vitamin a and immune regulation: role of retinoic acid in gut-associated dendritic cell education, immune protection and tolerance, Mol. Asp. Med. 33 (2012) 63–76.
[21] J. Maia, T. Santos, S. Aday, F. Agasse, L. Cortes, J.O. Malva, L. Bernardino, L. Ferreira, Controlling the neuronal differentiation of stem cells by the intracellular delivery of retinoic acid-loaded nanoparticles, ACS Nano 5 (2011) 97–106.
[22] P.D. Tonge, P.W. Andrews, Retinoic acid directs neuronal differentiation of human pluripotent stem cell lines in a non-cell-autonomous manner, Differentiation 80 (2010) 20–30.
[23] V.E. Morrison, V.N. Smith, J.K. Huang, Retinoic acid Is required for oligodendrocyte precursor cell production and differentiation in the postnatal mouse corpus callosum, eNeuro 7 (2020).
[24] B. Sivakumar, R.G. Aswathy, R. Romero-Aburto, T. Mitcham, K.A. Mitchel, Y. Nagaoka, R.R. Bouchard, P.M. Ajayan, T. Maekawa, D.N. Sakthikumar, Highly versatile SPION encapsulated PLGA nanoparticles as photothermal ablators of cancer cells and as multimodal imaging agents, Biomater. Sci. 5 (2017) 432–443.
[25] L. Nuñez-Magos, J. Lira-Escobedo, R. Rodríguez-López, M. Muñoz-Navia, F. Castillo-Rivera, P.X. Viveros-Méndez, E. Araujo, A. Encinas, S.A. Saucedo-Anaya, S. Aranda-Espinoza, Effects of DC magnetic fields on magnetoliposomes, Front. Mol. Biosci. 8 (2021), 703417.
[26] K. Messaoudi, P. Saulnier, K. Boesen, J.P. Benoit, F. Lagarce, Anti-epidermal growth factor receptor siRNA carried by chitosan-transacylated lipid nanocapsules increases sensitivity of glioblastoma cells to temozolomide, Int. J. Nanomedicine 9 (2014) 1479–1490.
[27] Y. Labrak, B. Heurtault, B. Frisch, P. Saulnier, E. Lepeltier, V.E. Miron, G. G. Muccioli, A. des Rieux, Impact of anti-PDGFRα antibody surface functionalization on LNC uptake by oligodendrocyte progenitor cells, Int. J. Pharm. 618 (2022), 121623.
[28] M. Talelli, C.J.F. Rijcken, T. Lammers, P.R. Seevinck, G. Storm, C.F. van Nostrum, W.E. Hennink, Superparamagnetic iron oxide nanoparticles encapsulated in biodegradable thermosensitive polymeric micelles: toward a yargeted nanomedicine suitable for image-guided drug delivery, Langmuir 25 (2009) 2060–2067.
[29] Y. Chen, V. Balasubramaniyan, J. Peng, E.C. Hurlock, M. Tallquist, J. Li, Q.R. Lu, Isolation and culture of rat and mouse oligodendrocyte precursor cells, Nat. Protoc. 2 (2007) 1044–1051.
[30] K.D. McCarthy, J. de Vellis, Preparation of separate astroglial and oligodendroglial cell cultures from rat cerebral tissue, J. Cell Biol. 85 (1980) 890–902.
[31] A. ISO 10993-5, 2009 Biological Evaluation of Medical Devices-Part 5: Tests for in Vitro Cytotoxicity Vol. 2007, ISO, Phoenix, USA, 2009, pp. 1–11.
[32] P. Kumar, A. Nagarajan, P.D. Uchil, Analysis of cell viability by the alamar blue assay, Cold Spring. Harb. Protoc. 2018 (2018).
[33] F. Bouçanova, A.F. Maia, A. Cruz, V. Millar, I. Mendes Pinto, J.B. Relvas, H. S. Domingues, Collar occupancy: a new quantitative imaging tool for morphometric analysis of oligodendrocytes, J. Neurosci. Methods 294 (2018) 122–135.
[34] L. Martínez-Jothar, S. Doulkeridou, R.M. Schiffelers, J. Sastre Torano, S. Oliveira, C.F. van Nostrum, W.E. Hennink, Insights into maleimide-thiol conjugation chemistry: conditions for efficient surface functionalization of nanoparticles for receptor targeting, J. Control. Release. 282 (2018) 101–109.

[35] B. Heurtault, P. Saulnier, B. Pech, M.-C. Venier-Julienne, J.-E. Proust, R. Phan-Tan-Luu, J.-P. Benoît, The influence of lipid nanocapsule composition on their size distribution, Eur. J. Pharm. Sci. 18 (2003) 55–61.
[36] M. Shilo, A. Sharon, K. Baranes, M. Motiei, J.-P.M. Lellouche, R. Popovtzer, The effect of nanoparticle size on the probability to cross the blood-brain barrier: an in-vitro endothelial cell model, J. Nanobiotechnol. 13 (2015) 19.
[37] S. Ohta, E. Kikuchi, A. Ishijima, T. Azuma, I. Sakuma, T. Ito, Investigating the optimum size of nanoparticles for their delivery into the brain assisted by focused ultrasound-induced blood–brain barrier opening, Sci. Rep. 10 (2020) 18220.
[38] Q. Meng, H. Meng, Y. Pan, J. Liu, J. Li, Y. Qi, Y. Huang, Influence of nanoparticle size on blood–brain barrier penetration and the accumulation of anti-seizure medicines in the brain, J. Mater. Chem. B 10 (2022) 271–281.
[39] P.J. Kennedy, F. Sousa, D. Ferreira, C. Pereira, M. Nestor, C. Oliveira, P.L. Granja, B. Sarmento, Fab-conjugated PLGA nanoparticles effectively target cancer cells expressing human CD44v6, Acta Biomater. 81 (2018) 208–218.
[40] A. Lamprecht, Y. Bouligand, J.-P. Benoit, New lipid nanocapsules exhibit sustained release properties for amiodarone, J. Control. Release 84 (2002) 59–68.
[41] J. Aparicio-Blanco, I.A. Romero, D.K. Male, K. Slowing, L. García-García, A. I. Torres-Suárez, Cannabidiol enhances the passage of lipid nanocapsules across the blood-brain barrier both in vitro and in vivo, Mol. Pharm. 16 (2019) 1999–2010.
[42] G. Bastiat, C.O. Pritz, C. Roider, F. Fouchet, E. Lignières, A. Jesacher, R. Glueckert, M. Ritsch-Marte, A. Schrott-Fischer, P. Saulnier, J.P. Benoit, A new tool to ensure the fluorescent dye labeling stability of nanocarriers: a real challenge for fluorescence imaging, J. Control. Release 170 (2013) 334–342.
[43] R. Takamura, N. Watamura, M. Nikkuni, T. Ohshima, All-trans retinoic acid improved impaired proliferation of neural stem cells and suppressed microglial activation in the hippocampus in an Alzheimer's mouse model, J. Neurosci. Res. 95 (2017) 897–906.
[44] J. Hellmann-Regen, G. Kronenberg, R. Uhlemann, D. Freyer, M. Endres, K. Gertz, Accelerated degradation of retinoic acid by activated microglia, J. Neuroimmunol. 256 (2013) 1–6.
[45] M. Machado-Pereira, T. Santos, L. Ferreira, L. Bernardino, R. Ferreira, Anti-inflammatory strategy for M2 microglial polarization using retinoic acid-loaded nanoparticles, Mediat. Inflamm. 2017 (2017) 6742427.
[46] A. Mwema, P. Bottemanne, A. Paquot, B. Ucakar, K. Vanvarenberg, M. Alhouayek, G.G. Muccioli, A. des Rieux, Lipid nanocapsules for the nose-to-brain delivery of the anti-inflammatory bioactive lipid PGD2-G, Nanomedicine 48 (2023), 102633.
[47] D. Drescher, T. Büchner, P. Schrade, H. Traub, S. Werner, P. Guttmann, S. Bachmann, J. Kneipp, Influence of nuclear localization sequences on the intracellular fate of gold nanoparticles, ACS Nano 15 (2021) 14838–14849.
[48] C. Martins, F. Araújo, M.J. Gomes, C. Fernandes, R. Nunes, W. Li, H.A. Santos, F. Borges, B. Sarmento, Using microfluidic platforms to develop CNS-targeted polymeric nanoparticles for HIV therapy, Eur. J. Pharm. Biopharm. 138 (2019) 111–124.
[49] B. Weksler, I.A. Romero, P.-O. Couraud, The hCMEC/D3 cell line as a model of the human blood brain barrier, Fluids Barriers CNS 10 (2013) 16.
[50] M.S. Thomsen, K.B. Johnsen, K. Kucharz, M. Lauritzen, T. Moos, Blood-brain barrier transport of transferrin receptor-targeted nanoparticles, Pharmaceutics 14 (2022).
[51] D.T. Wiley, P. Webster, A. Gale, M.E. Davis, Transcytosis and brain uptake of transferrin-containing nanoparticles by tuning avidity to transferrin receptor, Proc. Natl. Acad. Sci. U. S. A. 110 (2013) 8662–8667.
[52] C. Luo, C. Jian, Y. Liao, Q. Huang, Y. Wu, X. Liu, D. Zou, Y. Wu, The role of microglia in multiple sclerosis, Neuropsychiatr. Dis. Treat. 13 (2017) 1661–1667.
[53] M.T. Haindl, U. Köck, M. Zeitelhofer-Adzemovic, F. Fazekas, S. Hochmeister, The formation of a glial scar does not prohibit remyelination in an animal model of multiple sclerosis, Glia 67 (2019) 467–481.
[54] C.U.A. Kloss, M. Bohatschek, G.W. Kreutzberg, G. Raivich, Effect of lipopolysaccharide on the morphology and integrin immunoreactivity of ramified microglia in the mouse brain and in cell culture, Exp. Neurol. 168 (2001) 32–46.
[55] V. Clemens, F. Regen, N. Le Bret, I. Heuser, J. Hellmann-Regen, Retinoic acid enhances apolipoprotein E synthesis in human macrophages, J. Alzheimers Dis. 61 (2018) 1295–1300.
[56] J.S. Mathew, R.P. Sharma, Effect of all-trans-retinoic acid on cytokine production in a murine macrophage cell line, Int. J. Immunopharmacol. 22 (2000) 693–706.
[57] S. Li, Y. Lei, J. Lei, H. Li, All-trans retinoic acid promotes macrophage phagocytosis and decreases inflammation via inhibiting CD14/TLR4 in acute lung injury, Mol. Med. Rep. 24 (2021) 868.
[58] J. Xu, P.D. Drew, 9-Cis-retinoic acid suppresses inflammatory responses of microglia and astrocytes, J. Neuroimmunol. 171 (2006) 135–144.
[59] S. Kuhn, L. Gritti, D. Crooks, Y. Dombrowski, Oligodendrocytes in development, myelin generation and beyond, Cells 8 (2019).
[60] M.B. Goncalves, Y. Wu, E. Clarke, J. Grist, C. Hobbs, D. Trigo, J. Jack, J.P. T. Corcoran, Regulation of myelination by exosome associated retinoic acid release from NG2-positive cells, J. Neurosci. 39 (2019) 3013–3027.
[61] J.K. Huang, A.A. Jarjour, B. Nait Oumesmar, C. Kerninon, A. Williams, W. Krezel, H. Kagechika, J. Bauer, C. Zhao, A. Baron-Van Evercooren, P. Chambon, C. Ffrench-Constant, R.J.M. Franklin, Retinoid X receptor gamma signaling accelerates CNS remyelination, Nat. Neurosci. 14 (2011) 45–53.
[62] M.S. Natrajan, A.G. de la Fuente, A.H. Crawford, E. Linehan, V. Nuñez, K. R. Johnson, T. Wu, D.C. Fitzgerald, M. Ricote, B. Bielekova, R.J. Franklin, Retinoid X receptor activation reverses age-related deficiencies in myelin debris phagocytosis and remyelination, Brain 138 (2015) 3581–3597.
[63] P. Laeng, D. Décimo, B. Pettmann, T. Janet, G. Labourdette, Retinoic acid regulates the development of oligodendrocyte precursor cells in vitro, J. Neurosci. Res. 39 (1994) 613–633.
[64] S.y. Kim, E.E. Kelland, J.h. Kim, B.T. Lund, X. Chang, K. Wang, L.P. Weiner, The influence of retinoic acid on the human oligodendrocyte precursor cells by RNA-sequencing, Biochem. Biophys. Rep. 9 (2017) 166–172.
[65] I. Osorio-Querejeta, S. Carregal-Romero, A. Ayerdi-Izquierdo, I. Mäger, A. Egimendia Wood, M. Betanzos, A. Alberro, L. Iparraguirre, L. Moles, I. Llarena, M. Möller, F. Goñi-de-Cerio, G. Bijelic, P. Ramos-Cabrer, M. Muñoz-Culla, D. Otaegui, MiR-219a-5p enriched extracellular vesicles induce OPC differentiation and EAE improvement more efficiently than liposomes and polymeric nanoparticles, Pharmaceutics 12 (2020).